Multi-century impacts of ice retreat on sea level and tides in Hudson Bay

Anna-Mireilla Hayden

Department of Earth and Planetary Sciences

McGill University

Montréal, Quebec

February 2019

A thesis submitted to McGill University in partial fulfillment of the requirements of the degree of Master of Science

Table of Contents

Acknowledgements

First and foremost, I would like to extend my sincerest thanks to my supervisor, Dr. Natalya Gomez for her continual support and steadfast encouragement throughout my Master's. Natalya's vast knowledge enkindled my desire to learn more and take action through research.

Special thanks to my collaborators and colleagues. Among these, I wish to thank especially Sophie-Berenice Wilmes, Mattias Green, Linda Pan, Holly Han, and Nick Golledge whose comments and insight helped to shape this thesis. I am thankful for the financial support for this project provided by NSERC and Québec-Océan.

I would like to thank all members of the Gomez Geodynamics Group (GGG!), past and present, for enriching my experience as a graduate student. In particular, thank you to Erik Chan, Holly Han, Dave Purnell, Linda Pan, and Jeannette Wan, for their companionship and enthusiasm.

I would also like to express my deepest appreciation to Dr. Jeffrey McKenzie, who offered unwavering guidance and valuable advice, especially when graduate school was particularly "tidal".

I am extremely grateful to Dr. William Minarik, who has served as a mentor throughout my undergraduate and graduate studies.

I have been privileged to have studied under the supervision of Dr. Bruno Tremblay during my Master's. I am thankful for his wisdom, time, and for reassuring me throughout my studies.

Anne, Kristy, and Angela: Thank you for all your assistance and hard work in keeping our department running smoothly.

I am incredibly grateful for all the love and support from my family: Mom, Angelisa, Mama, Papa, and Randy – thank you for always believing in me and for providing endless encouragement throughout my studies.

Frédéric, thank you for reminding me to stay positive, for your patience and company while I would work long nights and weekends on this thesis, and for enthusiastically joining me on any adventure I suggested.

I dedicate this thesis to my papa, my north star, Dr. John Terry Dennis. I am inspired by his grit, patience, love, and zest for life. His curiosity in my academic endeavours provided me

with an invaluable outlet for scientific expression, without which I would have not been able to complete this thesis.

Contribution of Authors

The following thesis presents original research conducted by the author at the Department of Earth and Planetary Sciences at McGill University, under the supervision of Dr. Natalya Gomez. This thesis is presented as a manuscript submitted for publication in the peer-reviewed *Journal of Geophysical Research: Oceans*. The author is the primary contributor to the data analysis and writing and is listed as first author. The manuscript is entitled "Multi-century impacts of ice sheet retreat on sea level and tides in Hudson Bay" and is co-authored by Natalya Gomez, Sophie-Berenice Wilmes, Mattias Green, Linda Pan, Holly Han, and Nicholas R. Golledge. All co-authors have contributed intellectually to the modelling, analysis, interpretation of data, and writing and proofreading of the manuscript.

List of Figures

List of Tables

Abstract

Sea level change associated with ongoing and future melting of the Greenland and Antarctic Ice Sheets is one of the most threatening consequences of anthropogenic climate change and will greatly impact low-lying coastal communities. Regional sea level changes associated with changes in grounded ice mass can differ significantly from the globally averaged value due to gravitational, rotational, and Earth deformational effects. In addition to contemporary changes in the current polar ice sheets, past changes in ice sheet configurations over the last glacial cycle also contribute significantly to regional trends in sea level. This is especially true in the case of Hudson Bay, a shallow inland sea in northern Canada that was ice covered at the Last Glacial Maximum leading to ongoing crustal uplift and sea level fall of up to 1cm/year in the modern. It remains to be seen whether this trend will continue in the coming centuries as the polar ice sheets retreat because it is unclear what the dominant contributor to sea level change in the Hudson Bay will be, or even what the sign will be. Sea level changes in turn affect tidal dynamics due to the sensitivity of tides to water depth, and recent work has suggested that future sea level changes as a consequence of ice sheet collapse will impact tides globally. However, previous studies on both modern and future tides have been unable to accurately model tides in Hudson Bay due to large uncertainties in bathymetry in the bay.

This thesis addresses the aforementioned knowledge gaps and quantifies the impact of past and future ice sheet retreat on sea level and tides in the Hudson Bay region. In Chapter 1, I outline the background theory on sea level and tides. In Chapter 2, I present a paper, submitted to *Journal of Geophysical Research: Oceans*, in which coauthors and I model sea level changes over the next 500 years associated with the combined effects of ongoing glacial isostatic adjustment and future ice loss from the Greenland and Antarctic Ice Sheets and the resulting changes in ocean tides in Hudson Bay. To establish an initial condition for the simulations, we investigate the accuracy of current bathymetry datasets in reproducing modern ocean tides measured from satellite observations. We produce a new, improved bathymetry dataset in the bay constrained, for the first time, using tide observations. It is shown that the Antarctic ice loss scenario considered determines the sign and magnitude of sea level and tide changes in the Hudson Bay region, with the largest changes projected in the adjacent Hudson Strait. Furthermore, it is demonstrated that future sea level rise would greatly affect tidal energy dissipation in the region, which could have significant and widespread impacts on the global

tidal energy balance. Chapter 3 concludes this thesis with a discussion and recommendations for future directions of research and the consequences of our results on navigation, ecosystems, and societies.

Résumé

Les variations du niveau de la mer, causées par la fonte actuelle et future des inlandsis au Groenland et en Antarctique, sont l'une des conséquences les plus graves des changements climatiques anthropiques, et auront un impact considérable sur les communautés de basses-terres côtières. Les variations régionales du niveau de la mer, associées aux changements dans la masse des glaces ancrées, peuvent significativement différer de la valeur moyenne globale en raison des effets gravitationnels, rotationnels, et de la déformation de la Terre. En plus des changements actuels concernant les inlandsis polaires, les transformations passées au sujet des configurations des inlandsis lors de la période glaciaire précédente, ont aussi significativement contribuées aux variabilités régionales du niveau de la mer. Ceci est particulièrement vrai dans le cas de la Baie d'Hudson, une mer intérieure peu profonde au nord du Canada qui était recouverte de glace pendant le dernier maximum glaciaire, entrainant un rebond post-glaciaire continu et une baisse du niveau de la mer jusqu'à 1cm/an actuellement. Il reste à voir si cette tendance se poursuivra au cours des prochains siècles alors que les inlandsis polaires se retirent. Ainsi, il n'est pas clairement établi quel sera le principal facteur de variation du niveau de la mer dans la Baie d'Hudson, ni même quel sera le signe. Les variations du niveau de la mer ont à leur tour une incidence sur la dynamique des marées en raison de la sensibilité des marées par rapport à la profondeur d'eau; une étude récente a suggéré que les variations futures du niveau de la mer, résultant de l'effondrement des inlandsis, auront un impact sur les marées à l'échelle mondiale. Cependant, des études antérieures sur les marées présentes et futures n'ont pas permis de modéliser avec exactitude les marées dans la Baie d'Hudson, et cela en raison des grandes incertitudes entourant la bathymétrie de la baie.

Cette thèse aborde les manques de connaissances susmentionnés et quantifie l'impact du recul des inlandsis passés et futurs sur le niveau de la mer et les marées de la région de la Baie d'Hudson. Le chapitre 1 présente le contexte théorique sur le niveau de la mer et des marées. Le chapitre 2 présente un article soumis au *Journal of Geophysical Research: Oceans*, dans lequel les co-auteurs et moi-même modélisons les variations du niveau de la mer au cours des 500 prochaines années qui sont associées à l'effet combiné d'ajustement glaciaire isostatique en cours et à la future perte de glace des inlandsis du Groenland et de l'Antarctique, ainsi que les changements qui en découlent concernant les marées de la Baie d'Hudson. Afin d'établir une condition initiale pour des simulations, nous examinons l'exactitude des données actuelles de

bathymétrie en reproduisant les marées océaniques actuelles mesurées à partir d'observations satellites. Nous produisons un nouvel ensemble de données bathymétriques amélioré, contraint pour la première fois en utilisant les observations des marées. Il est démontré que le scénario considéré de perte de glace en Antarctique détermine le signe et la magnitude des variations du niveau de la mer et des marées dans la région de la Baie d'Hudson, les plus importantes étant projetées dans le Détroit d'Hudson adjacent. De plus, il est démontré que la hausse future du niveau de la mer aurait une incidence importante sur la dissipation de l'énergie des marées dans la région, ce qui pourrait avoir des effets importants et répandus sur l'équilibre mondial de l'énergie des marées. Le chapitre 3 conclut cette thèse avec une discussion et des recommandations sur les orientations futures de recherche et les conséquences de nos résultats sur la navigation, les écosystèmes et les sociétés.

1. **Introduction**

1.1 Spatially variable sea level changes

Sea level changes occur over a large range of temporal scales, from sub-daily (e.g. tides) to millions of years (e.g. mantle convection). In the coming centuries, future global mean sea level changes are expected to be dominated by contributions from the Greenland and Antarctic Ice Sheets (Church et al., 2013). However, the resulting pattern of sea level change associated with melting ice sheets is far from uniform and exhibits significant geographical variability (Clark & Lingle, 1977; Gomez et al., 2010; Mitrovica et al., 2001; Woodward, 1888). To appreciate and understand why such patterns emerge, this section begins with a discussion on the physics of sea level change associated with surface mass (ice and water) loading redistribution. Next, I present an overview of sea level changes in Hudson Bay. This section concludes with a discussion of the Representative Concentration Pathway framework for predicting future sea level change.

1.1.1 Sea level theory

In this section, I describe the sea level equation that includes migrating shorelines, Earth rotation and deformation of the solid Earth. A complete derivation of the sea level equation is available in Gomez et al. (2010) and Mitrovica et al. (2011).

It is first necessary to define the usage of relative sea level (SL). Relative sea level is defined as the difference between the height of the ocean surface equipotential, or geoid, G, and the solid earth surface, R, at a specific colatitude (θ) and colongitude (ψ) at time t:

$$SL(\theta, \psi, t) = G(\theta, \psi, t) - R(\theta, \psi, t) \tag{1}$$

The total change in the globally defined sea level ΔSL at time t_j can be calculated as:

$$\Delta SL(\theta, \psi, t_j) = \Delta G(\theta, \psi, t_j) - \Delta R(\theta, \psi, t_j) \tag{2}$$

SL is defined at every location on the globe. Topography (T) is then defined as the negative of relative sea level (SL), i.e. the elevation of the land is negative sea level:

$$T(t) = -SL(t) \tag{3}$$

Conversely, ocean height (S) is only defined over the oceans. To obtain S, SL is projected onto the ocean function, C^*, which defines the regions where oceans are present:

$$C^* = \begin{cases} 1, & if\ SL > 0\ and\ there\ is\ no\ grounded\ ice \\ 0, & elsewhere \end{cases} \tag{4}$$

With these terms defined, we can introduce the sea level equation that accounts for shoreline migration. For a given location and time t_j, the change in ocean height ΔS is defined as the change in sea level (ΔSL) projected onto the ocean function minus the topography T projected onto the change in the ocean function:

$$\Delta S(\theta, \psi, t_j) = \Delta SL(\theta, \psi, t_j) * C^*(\theta, \psi, t_j) - T(\theta, \psi, t_0)\left[C^*(t_j) - C^*(t_0)\right] \tag{5}$$

The first term, $\Delta SL(\theta, \psi, t_j) * C^*(\theta, \psi, t_j)$ describes the change in the ocean depth. The term $T(\theta, \psi, t_0)\left[C^*(t_j) - C^*(t_0)\right]$ accounts for shoreline migration. Here, the shoreline is defined at the location where sea level and topography are equal to each other, such that both topography and sea level equal 0. Shoreline migration refers to the lateral movement of the ocean boundary, and can be landwards as sea level rises, or oceanwards as sea level falls.

The ΔG term of ΔSL can be further decomposed into uniform shift (hereafter $\frac{\Delta\Phi}{g}$, where $\Delta\Phi$ is the perturbation to the equipotential and g is the acceleration due to gravity) and geographically variable (hereafter $\Delta\mathcal{G}$) components. The uniform shift component describes the change in the height of the equipotential on which the ocean surface lies, such that the ocean surface at a later time t_j lies on a different equipotential compared to $t = 0$. The uniform shift component is calculated by applying the principle of conservation of mass (i.e. a decrease in ice sheet mass will result in an increase in ocean mass). The interpretation of the uniform shift in

equipotential is as follows: while the sea surface is assumed to be constrained to an equipotential surface, over time, the location of this equipotential surface can change as mass is exchanged between the ice sheets and the oceans. $\Delta\mathcal{G}$ describes the perturbation to the uniform shift that arises because of the changes in the gravitational attraction between ice and oceans. ΔG can then be written as:

$$\Delta G(\theta, \psi, t_j) = \Delta\mathcal{G}(\theta, \psi, t_j) + \frac{\Delta\Phi_{t_j}}{g} \tag{6}$$

and ΔSL:

$$\Delta SL(\theta, \psi, t_j) = \Delta\mathcal{SL}(\theta, \psi, t_j) + \frac{\Delta\Phi_{t_j}}{g} \tag{7}$$

where $\Delta\mathcal{SL}$ is the geographically variable component of SL. Changes in $\Delta\mathcal{SL}$ are a function of changes in grounded ice (ΔI) and ocean height (ΔS), in addition to changes in the angular velocity of Earth ($\Delta\omega$). Redistributing the mass of the ice sheets and oceans changes the equipotential on which the ocean height (S) lies, and this redistribution deforms the planet, which feeds back into changes in the ocean surface equipotential. With the geographical dependency implicitly present, the generalized sea level equation can be succinctly written as (see Gomez et al., 2010 and Mitrovica et al., 2011, for intermediate steps):

$$\Delta S(t_j) = \left[\Delta\mathcal{SL}(\Delta\mathrm{I}, \Delta\mathrm{S}, \Delta\omega, t_j) + \frac{\Delta\Phi(t_j)}{g}\right] * C^*(t_j) - T(t_0)\left[C^*(t_j) - C^*(t_0)\right] \tag{8}$$

1.1.2 The sea level model and sea level fingerprints

When an ice sheet melts, sea level does not rise uniformly across the globe. Regional sea level changes can differ substantially from the global mean sea level change, producing distinct patterns or "fingerprints" of sea level rise and fall (e.g., Mitrovica et al., 2011). These deviations are due to spatial variability in gravitational, solid Earth deformational, and Earth rotational effects, in addition to changes in ocean dynamics. The following section describes the first three of these effects, as they are included in the sea level model used in this thesis.

Ice sheets are large enough to exert a gravitational attraction on the water surrounding them. When ice mass accumulates, there is an increased gravitational attraction exerted by the

ice, causing sea level to rise close to the location of increased mass, while further away sea level falls. Conversely, when ice mass is lost, the weakened gravitational attraction next to the ice sheet results in a local sea level fall. At greater distances from the source of ice loss, the sea level rise is higher than the global average, such that mass is conserved (Tamisiea & Mitrovica, 2011).

The solid Earth is not completely rigid and yields to mass that is added to its surface, this effect is known as the Earth deformational effect (Gomez et al., 2010; Mitrovica et al., 2009; Tamisiea & Mitrovica, 2011). In terms of ice sheets and sea level, this is commonly referred to as ice and ocean loading. An increase in the mass of the ice load depresses the solid Earth below. In response to a loss of ice mass, the solid Earth underlying the former ice load begins to rebound, seeking equilibrium. The solid Earth responds elastically on short timescales, that is, the land under and adjacent to the waning ice sheet responds instantaneously once the ice load is removed, and the land rises relative to the ocean. The elastic response to loading changes is important when considering present day ice loss. Furthermore, the Earth has a memory of the removal of ice sheets, resulting in the viscous response of the solid Earth over glacial timescales. Thus, the solid Earth must be modeled as a viscoelastic body when considering the effects of ice loss on sea level.

The redistribution of mass also affects the orientation of the Earth's rotation axis relative to the Earth's surface geography, this effect is known as true polar wander (TPW) (Milne & Mitrovica, 1998; Mitrovica & Milne, 2003; Kendall et al., 2005). With ice sheet growth, the rotation axis will move away from the ice load in order to conserve angular momentum. Conversely, when an ice sheet melts, the redistribution of mass orients the rotation axis towards where the load once was (Gomez et al., 2010). The perturbation in the rotation axis results in two quadrants of the Earth experiencing an accentuated sea level rise, and two quadrants experiencing a sea level fall (Gomez et al., 2010; Mitrovica et al., 2009). For Greenland ice loss, this translates to a large sea level rise in the South Atlantic and Northwest Pacific (Tamisiea & Mitrovica, 2011). Under West Antarctic melting, the rotational feedback results in an accentuated sea level rise along the coasts of North America and in the Indian Ocean (Gomez et al., 2010; Mitrovica et al., 2009; Mitrovica & Tamisiea, 2011).

1.1.3 Past and present sea level changes in the Hudson Bay

During the Pleistocene epoch, defined here as 2,600,000 – 11,700 years before present (yr B.P.), changes in the Earth's climate between colder and warmer periods lead to the growth and decline, respectively, of continental-sized ice sheets. When the climate is cooler (warmer), the climate is in a glacial (interglacial) period, and there is more (less) water stored in continental ice sheets and global sea levels are lower (higher). During the Last Glacial Maximum (LGM, 21,000 – 18,000 yr B.P.), sea levels were 120-130 m lower than present day (Clark et al., 2009), with two ice sheets covering northern Canada: the Laurentide Ice Sheet and the Innutian Ice Sheet (Dyke, 2004). At the Laurentide Ice Sheet's maximum extent, ice 3-4 km thick covered the Hudson Bay region (Simon et al., 2016). Beneath the ice sheet and within the Earth's interior, hot mantle rock flowed downward and spread out laterally, resulting in depression of the Earth's crust. At the periphery of the ice sheet, the land rose in response to the outwardly flowing mantle material **(**Figure 1a).

Throughout the early Holocene (9,000 – 6,000 yr B.P.), radiocarbon dates indicate that the Laurentide Ice Sheet was retreating extensively (Dyke, 2004). By ~ 7,000 yr B.P., the Laurentide Ice Sheet had melted (Denton et al., 2010) and the process of subsiding and rising land reversed itself (Figure 1b). Land under the former ice sheet began to rise, and the peripheral regions began to subside. The influx of meltwater from the rapid retreat of the ice flooded the surrounding land beyond the current shorelines of present-day Hudson Bay, creating the Tyrrell Sea (~7,000 yr B.P.; Lee, 1960). As the land continued to rise, the Tyrell Sea drained to form the present Hudson Bay and James Bay.

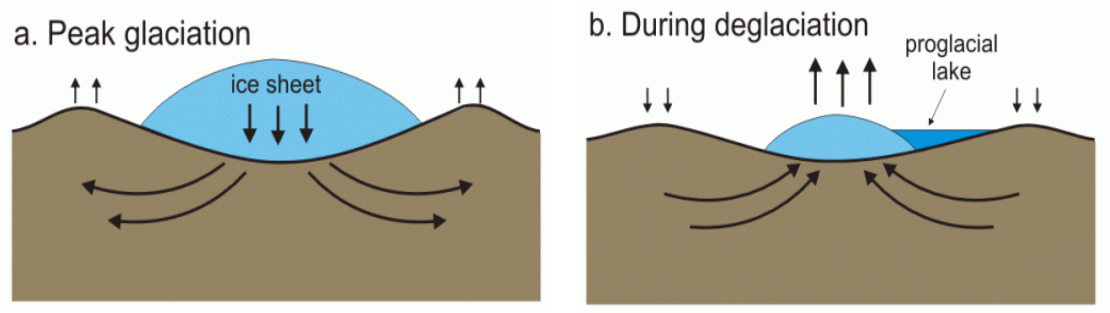

Figure 1: Schematic showing solid Earth deformation during glaciations and interglacials. a) Solid Earth subsidence and rebound due to ice loading during glacial periods. The solid Earth below the ice sheet is depressed and the mantle flows downwards and spreads out laterally. At the peripheral regions, called forebulges, the land rises. b) Solid Earth subsidence and rebound due to ice loading during interglacial periods. The solid Earth below the former ice sheet rises and the forebulges collapse. Figure from Tom James, Natural Resources Canada.

The sequence of past ice-ocean mass exchanges yields an ongoing response of the solid earth to such loading changes, referred to as Glacial Isostatic Adjustment (GIA). This process is still occurring because the Earth's mantle behaves like a highly viscous fluid over long time scales. Therefore, all modern observations of sea level related quantities are impacted by past ice and ocean loading changes. In Hudson Bay, the rate of glacial isostatic uplift of the land is approximately 1 cm/year (Peltier, 1999). It follows that the tide gauge in Churchill, Manitoba, is also detecting the change in the relative sea level, as indicated by a relative long-term sea level fall (Figure 2).

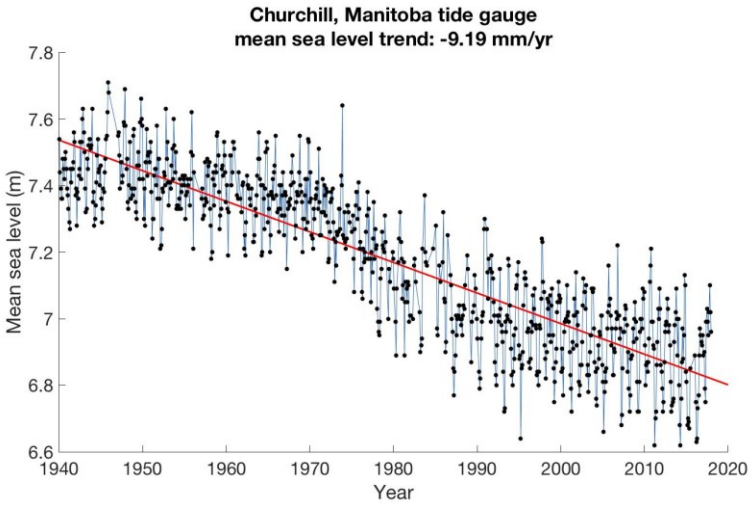

Figure 2: Relative sea level changes at Churchill, Manitoba. The black points show the measurements from the tide gauge station at Churchill, with the blue curve connecting the points, the red line indicates the mean trend. This figure illustrates the relative sea level fall through time as a response to vertical land motion due to past ice loading changes. Data from the Permanent Service for Mean Sea Level (PSMSL).

1.1.4 Representative Concentration Pathways

A growing body of evidence suggests that mass loss from the Greenland and Antarctic Ice Sheets has accelerated in recent decades (e.g. Chen et al., 2017; Forsberg et al., 2017), and in the coming centuries the polar ice sheets are expected to dominate sea level change (Church et al., 2013; Golledge et al., 2015, 2019). Since placing a bound on the future sea level rise due to ice loss is not a trivial task, it is beneficial to introduce a framework on which sea level projections are often based. In this section, I describe the Representative Concentration Pathways, as they guide in the simulations presented in Chapter 2.

Representative Concentration Pathways (RCPs), formulated by the Intergovernmental Panel on Climate Change (IPCC) (Moss et al., 2008; 2010), have served as the primary resource for climate change, and hence, sea level projections in recent years. Four RCPs indicate possible trajectories of future greenhouse gas concentrations and the associated increase in global mean surface temperature. On the low end of the spectrum, RCP2.6 assumes a peak in emissions by 2020, followed by a concerted effort to decrease emissions (Meinshausen et al., 2011; Moss et al., 2008; 2010). Under RCP2.6, the likely increase in global mean temperature by the end of the century is 1.9-2.3°C above pre-industrial (1850-1900) levels (Meinshausen et al., 2011; Moss et

al., 2008; 2010). Conversely, the emission-intensive RCP8.5 scenario represents steadily increasing greenhouse gas emissions throughout the twenty-first century, with an accompanying global mean temperature increase of 3.2-5.4°C above pre-industrial levels (Meinshausen et al., 2011; Moss et al., 2008; 2010).

While RCP scenarios presented in the IPCC's Fifth Assessment Report extend to 2100, the inertia of the climate system implies a multi-century, and possibly a multi-millennial commitment to climate change (Clark et al., 2016; DeConto & Pollard, 2016; Golledge et al., 2015, 2019). Extended Concentration Pathways (ECPs) were developed as a way to project the changes in greenhouse gas emissions until 2300 (Meinshausen et al., 2011). The framework for creating an ECP is based on the following three options, as per Meinshausen et al. (2011): 1) radiative forcing and concentration of greenhouse gas can be kept constant, 2) emissions can be reduced over time, 3) emissions can continue at a constant rate over time. For instance, in the emission-intensive RCP8.5, the corresponding ECP8.5 assumes constant emissions until 2150, followed by a smooth transition to stable concentrations after 2250 (Meinshausen et al., 2011, Table 3). However, Meinshausen et al. (2011) emphasize that ECPs are highly speculative. To that end, ECPs should not be interpreted as the definitive pathway that would succeed the corresponding RCP scenario. Rather, ECPs provide a range of concentrations and forcing pathways that can be used in climate models, and evolves as does our understanding of earth system processes and behaviours.

Greenland's contribution to sea level change is predominantly driven by surface mass balance, followed by ice discharge via icebergs (Church et al., 2013). Conversely, the dynamic response is expected to dominate sea level changes due to Antarctic ice loss, but the future contribution from Antarctica remain highly uncertain due to the lack of observations to constrain models and an incomplete description of ice sheet-ocean-atmosphere interactions in current models (Kopp et al. 2017; Moore et al., 2013; Wingham et al., 2009). As the processes responsible for ice loss from Greenland are more well understood than those for Antarctica, there is more agreement in the literature on Greenland's response to RCP scenarios, which fall within a likely range of 0.07-0.21 m of globally averaged sea level rise by 2100 in response to RCP8.5 (Church et al., 2013; Clark et al., 2015; Slangen et al., 2016). For Antarctica, estimates range from 0.1 m to 1.46 m of globally averaged sea level rise by the end of the current century under the RCP8.5 scenario (Golledge et al., 2015, 2019; Kopp et al., 2017). Recent work by Edwards et

al. (2019) suggests that the highest end Antarctic scenarios are less likely by 2100, but cannot be ruled out in the longer-term future. Despite the uncertainty, it is agreed upon that the amount of mass lost from Antarctica and the accompanying sea level change is highly dependent on the emission scenario (DeConto & Pollard, 2016; Kopp et al., 2017).

1.2 Tides

Tides are responsible for the daily, short term variability in sea level, with the daily rise and fall in water levels due to the gravitational attraction of the moon and sun. To place the current work in context, this section presents an introduction to the theory behind tides. I first discuss the properties of waves and tides. I then present an overview of the forces causing the tides, followed by a description of periodic tidal constituents. This section concludes with a discussion on tide modelling. Current knowledge of tides in Hudson Bay is discussed in detail in Chapter 2.

1.2.1 Properties of waves and tides

As tides are a form of wave, it is first necessary to discuss the properties that define a wave. There are three main properties that define a wave. Firstly, waves do not transport matter, only energy. Secondly, this energy is transferred through the medium the wave is travelling through. Therefore, water waves result in the transfer of energy through the medium of water but not the transfer of water itself. Thirdly, to prevent matter from being displaced, there must be a resisting force. For tide waves, gravity provides the restoring force through hydrostatic pressure.

Figure 3 illustrates the main features of a wave: wave crest, wave trough, amplitude, range, wavelength, period, and frequency. The crest of a wave is the highest point of the wave. In tidal studies, the crest is referred to as high water (HW). Conversely, the trough is the lowest point of the wave, and is referred to as low water (LW) in tidal studies. Tidal amplitude refers to the vertical distance from the equilibrium point of the wave (mean water level, MWL, for tidal studies) to either the crest or the trough, whereas tidal range measures the distance between the trough and the crest. The wavelength (λ) is the horizontal distance between two successive crests or troughs. Tidal period refers to the time elapsed between two successive wave crests or

troughs. The frequency of a wave is defined as the number of periods per unit time. For tides, the frequency is often expressed as angular speed, measured in degrees per hour.

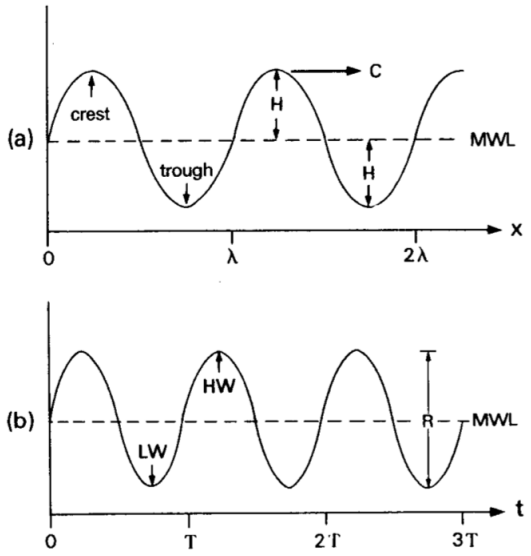

Figure 3: Terminology used to describe waves. Sinusoidal wave form as seen a) in space from an instant in time and b) at a fixed location over an interval in time. Figure from Forrester (1983).

Waves represent oscillations and can be either free or forced. Free oscillation means that there is no external force driving the back-and-forth motion, this is the natural frequency of the wave. Forced oscillations are those in which an external force plays a role in their generation. Tides are a type of forced oscillations, with the external force provided by the sun and moon's unbalanced gravitational attraction force.

A special form of oscillation in an ocean basin is that of ocean resonance. Resonance refers to the condition in which the driving and restoring forces within the system are mainly in unison, with the forcing frequency close to that of the natural frequency of the system. This produces a large amplitude response. Oscillations in the Bay of Fundy in New Brunswick and Ungava Bay in northern Quebec are close to resonance with the semi-diurnal M_2 tide (Forrester, 1983; Pugh & Woodworth, 2014). Resonance is dependent on the water depth, D, and the length, L, of the ocean basin. As represented in Equation 9, a long and/or shallow basin will have

a large natural period (T) of oscillation. However, this equation omits frictional effects, which becomes important in shallower water.

$$T = \frac{2L}{(gD)^{\frac{1}{2}}} \tag{9}$$

1.2.2 The tide generating forces

Tides are the ocean's response to the unbalanced gravitational attraction forces of the sun and moon. It is this unbalanced component of this force that results in the periodic rise and fall of water levels. Gravitational attraction between two bodies is represented by the Newton's Law of Gravitation. This law states that the net gravitational attraction force, F, separating two bodies is proportional to the product of the two masses and inversely proportional to the square of the distance separating the two bodies. Between the earth and moon, this can be written as:

$$F = G\frac{m_e m_l}{{R_l}^2} \tag{10}$$

Where m_e is the earth's mass, m_l is the moon's mass, R_l is the distance separating the two bodies center of mass, and G is the universal gravitational constant. Similarly, the gravitational attraction between the sun and earth can be obtained if instead the sun's mass and earth-sun center of mass distance is used.

The tide-generating force of the sun or of the moon is calculated as the difference between the gravitational attraction at their respective centres of mass and a point of interest on the earth's surface. Figure 4 illustrates the lunar tide generating force.

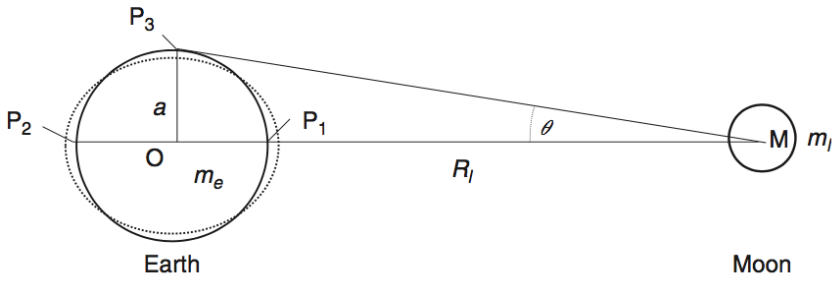

Figure 4: Diagram to show positions in the Earth–Moon system that are used to derive the tidal forces. The separation is distorted but the relative diameters of the Earth and Moon are to scale. Figure from Pugh & Woodworth (2014).

At a point on the earth facing away from the moon in the moon-earth system (P_2 in Figure 4), the gravitational attraction is smaller at this point than at the center of mass and water moves away from the moon. Mathematically, this is represented by:

$$F = G\frac{m_e m_l}{(R_l + a)^2} \tag{11}$$

where a is the radius of the earth and all other values are as previously defined. At a point on the earth facing the moon (P_1 in Figure 4), the strength of the gravitational force is stronger than at the center of mass, and the water is pulled towards the moon. This can be shown as:

$$F = G\frac{m_e m_l}{(R_l - a)^2} \tag{12}$$

Although the sun's mass is much greater than that of the moon, and hence has a larger gravitational pull on the earth, the tide generating force of the moon is approximately two times stronger than that of the sun. The tide generating force (F_t) varies inversely with the cube of the distance separating the two bodies, rather than the inverse square. The derivation for the earth-moon system at a point P_1 is presented here:

$$F_t = G\frac{m_e m_l}{(R_l - a)^2} - G\frac{m_e m_l}{{R_l}^2} \tag{13}$$

which can then be expanded to:

$$F_t = G m_e m_l \frac{2R_l a - a^2}{{R_l}^4 - 2a{R_l}^3 + {R_l}^2 a^2} \tag{14}$$

Since $R_l \gg a$, the expression can be simplified and rewritten as:

$$F_t = G m_e m_l \frac{2a}{{R_l}^3} \tag{15}$$

At P_2, the tide generating force can be written as:

$$F_t = -G m_e m_l \frac{2a}{{R_l}^3} \tag{16}$$

The net effect of the tide generating force produces two bulges, one on the side of the earth facing the moon, and the other on the side of the earth opposite the moon.

1.2.3 Harmonic Constituents

The precisely determined motions of the earth, sun, and moon and their frequencies enable tides to be analyzed and predicted with great certainty, as the tides are a consequence of these periodic motions. The description of tides can be decomposed mathematically into harmonic constituents based on the periodic fluctuations in the tide or tide raising force at a particular frequency.

An important distinction must be made regarding the day length and tidal period conventions. A solar day is 24 hours, and a lunar day is 24 hours and 50 minutes. The day lengths differ due to different reference points for measuring a complete rotation of the earth. A solar day represents the complete rotation of the earth with respect to the sun. A lunar day is a complete rotation of the earth with respect to the moon, it is longer than the solar day because by

the time the earth has completed a complete rotation, the moon has also revolved a small distance. The number of rise and fall cycles per lunar day is used to classify the tide. There are four main groups: semi-diurnal, diurnal, mixed; mainly semi-diurnal, and mixed; mainly diurnal:

1- Semi-diurnal: Characterized by two high water and two low water levels each lunar day. The magnitudes of the two low and two high water levels are approximately equal.
2- Diurnal: One high water and one low water each lunar day.
3- Mixed, mainly semi-diurnal: Two high water and two low water each day, but the magnitudes of the water levels are usually significantly different and are irregularly spaced throughout the lunar day.
4- Mixed, mainly diurnal: Sometimes two unequal high and low waters with irregular time spacing over the lunar day. Other times, there is only one high and low water during the lunar day.

The principal lunar semi-diurnal constituent, M_2, describes the motion of the earth relative to the moon. There are two high waters during the lunar day, with the period between the maxima equal to 12.42 hours. The angular speed of the M_2 constituent is therefore 360°/12.42hr = 28.984°/hr. The principal solar semi-diurnal constituent, S_2, describes the motion of the earth relative to the sun. There are two high waters during the solar day, with a period of 12.00 hours between the two maximums. The angular speed of this constituent is 360°/12.00hr = 30°/hr. When M_2 and S_2 align and are in phase, larger than average tidal ranges result (Figure 5a), and spring tides are observed. Spring tides occur during new and full moon. Conversely, when M_2 and S_2 are completely out of phase, smaller than average tidal ranges occur and neap tides are observed (Figure 5b), Neap tides correspond with the first and last quarters of the lunar cycle.

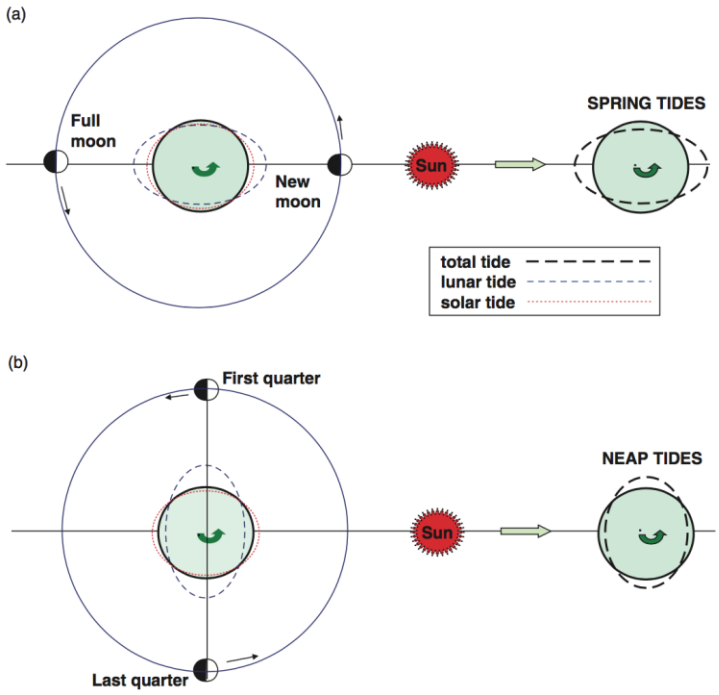

Figure 5: Spring–neap tidal cycles are produced by the relative motions of the Moon and Sun, at 14.8-day intervals. a) Spring tides occur at new and full moon, b) neap tides occur at the Moon's first and last quarter. Figure from Pugh & Woodworth (2014).

Due to the strong gravitational attraction associated with the moon and sun, M_2 and S_2 are known as the primary tidal constituents. However, these constituents are also influenced and modulated by other constituents with periods that are shorter and longer than a lunar or solar day. For example, since the orbits of the moon-earth and sun-earth systems are elliptical and at an angle to the earth's equator, the moon-earth and sun-earth separation distances and elevation angles change on several time scales, requiring additional constituents to be introduced. Furthermore, as the wave travels through shallow water, the influence of bottom morphology and friction becomes important for energy dissipation and the continued propagation of the wave (Pugh & Woodworth, 2014). To modulate the tidal wave through the shallower water, these interactions are represented by manipulating the astronomical tidal frequencies. Tidal constituents with shorter periods and occurring more often than semi-diurnally are referred to as overtides. The relative importance of each of these higher order constituents depends on the shape and topography of the basin (Pugh & Woodworth, 2014). To fully characterize tides at a

given location, an infinite combination of harmonic constituents would be required. In practice, however, a limited number of constituents are solved for.

1.2.4 Tide modelling

There are a number of tide models used to model past, present, and future tides. The various tide models can be differentiated by the data incorporated in the analysis. The different modelling schemes incorporate either: satellite altimetry data only, satellite altimetry data and/or tide gauge data, or forward tide models that calculate the tides from the hydrodynamic equations alone (Wilmes, 2016). This thesis presents results obtained using the Oregon State Tidal Inversion Software (OTIS, Egbert et al., 2004). Here, the governing equations in the OTIS model are described. A complete description of the OTIS model is available in Egbert et al. (2004), and the tide model setup used in Chapter 2 is outlined in Wilmes et al. (2017).

OTIS assimilates ocean depth and tidal current velocity observations to calculate the solution to the shallow water equations over a specific region. The shallow water equations describe a uniform density fluid that is in hydrostatic equilibrium bounded by topography at the bottom and a free surface from above. The governing equations of OTIS are:

$$\frac{\partial \mathbf{U}}{\partial t} + f \times \mathbf{U} = -gH\nabla\left(\zeta - \zeta_{EQ} - \zeta_{SAL}\right) - \mathbf{F} \tag{17}$$

$$\frac{\partial \zeta}{\partial t} = -\nabla \cdot \mathbf{U} \tag{18}$$

U is the depth integrated volume transport, calculated by multiplying the tidal current velocity u by the ocean depth, H. f is the Coriolis parameter and is equal to twice the Earth's angular rotation rate multiplied by the sine of the latitude, g is the gravitational constant, and t is time. ζ, ζ_{EQ}, and ζ_{SAL} are the tidal elevation, equilibrium tidal elevation, and self-attraction and loading elevations, respectively. Self-attraction and loading refers to the effect of redistributing mass on the Earth's surface, which deforms the solid Earth and affects the Earth's gravity field. This effect feeds back onto tides, changing the tidal elevation. **F** is the frictional losses due to bed friction, $\mathbf{F_b}$, and energy losses due to internal tide conversion, $\mathbf{F_{IT}}$. Bed friction can be expanded as:

$$\mathbf{F_b} = \frac{C_d \mathbf{u}|\mathbf{u}|}{H} \tag{19}$$

Where C_d is the drag coefficient and depends on the roughness of the bed, and $\mathbf{u}$ is the velocity vector for all tidal harmonic constituents included in the model.

2. Multi-century impacts of ice sheet retreat on sea level and ocean tides in Hudson Bay

Anna-Mireilla Hayden[1], Natalya Gomez[1], Sophie-Berenice Wilmes[2], Mattias Green[2], Linda Pan[1], Holly Han[1], Nicholas R. Golledge[3]

[1]Department of Earth and Planetary Sciences, McGill University, Montreal QC, Canada
[2]School of Ocean Sciences, Bangor University, Menai Bridge, Gwynedd, UK
[3]Victoria University of Wellington, Antarctic Research Centre, Wellington, New Zealand

2.1 Abstract

Past and modern large-scale ice sheet loss results in geographically variable sea level changes. At present, in Hudson Bay, Canada, sea level is decreasing due to glacial isostatic adjustment which represents a departure from the globally averaged sea level rise. However, large uncertainties over the sign and magnitude of the sea level trends with further polar ice sheet retreat in the coming centuries exist. Sea level changes affect ocean tides considerably, because tides are highly sensitive to changes in bathymetry. Here, we present multi-century sea level projections associated with a suite of past and future ice loss scenarios and consider the impact of these changes on ocean tides using an established tidal model. Modern tides in Hudson Bay are poorly resolved due to large uncertainties in bathymetry. To establish an initial condition for our simulations, we constrain bathymetry in the bay, for the first time, using tide observations. Due to gravitational, Earth rotational and deformational effects, Greenland ice loss will produce a small sea level fall in the bay, while Antarctic ice loss will produce a larger than average sea level rise. Our results show that the response of the Antarctic Ice Sheet to climate change strongly impacts the magnitude and sign of future sea level and tidal amplitude changes, with the largest changes predicted in Hudson Strait. We emphasize that further constraints on bathymetry and accurate projections of sea level and tides in Hudson Bay are imperative for assessing associated impacts on coastal communities and ecosystems.

2.2 Plain Language Summary

Hudson Bay is a shallow bay in northern Canada surrounded by coastal communities and ecosystems that are vulnerable to future sea level change. Hudson Bay was ice covered 21kys ago, and sea level is currently falling in the bay due to ongoing uplift of the land since the ice retreated. It is unclear if this trend will continue as the Greenland and Antarctic Ice Sheets melt, contributing to geographically variable sea level changes. Sea level changes also impact tides due to their sensitivity to water depth. We model future sea level and tide changes in Hudson Bay associated with uplift of the land, Greenland ice loss, and low- and high-end projections of Antarctic ice loss over the next 500 years. We show that sea level continues to fall under low-end Antarctic ice loss, and tidal amplitudes decrease. With rapid retreat of the Antarctic Ice Sheet, water depths in Hudson Bay could increase by 20% by 2500 and tidal amplitudes could change by up to half a meter. A better understanding of the response of Antarctica to climate change will improve projections of sea level and tide changes in the Arctic and the associated societal and environmental impacts.

2.3 Key Points

- The magnitude and sign of future sea level and tide changes in Hudson Bay depends on the evolution of the Antarctic Ice Sheet.
- Under rapid Antarctic ice loss, a 20% increase in water depths and up to 0.5 m changes in M_2 amplitudes could occur in Hudson Bay by 2500.
- We create a composite bathymetry that improves modelled tide solutions in Hudson Bay.

2.4 Introduction

Global mean sea level rise has accelerated in recent decades (Chen et al., 2017; Hay et al., 2015; Nerem et al., 2018), and this acceleration is expected to continue as global temperatures rise, resulting in thermal expansion of the oceans and melting of mountain glaciers and the polar ice sheets (Church et al., 2013; Clark et al., 2015; Slangen et al., 2016). Of these contributors, the Greenland and Antarctic ice sheets hold the largest potential to increase global mean sea level (WRCP Sea Level Working Group, 2018), and are expected to be the dominant contributors to global mean sea level rise on multi-century timescales (Church et al., 2013; Golledge et al., 2015). Regional sea level changes associated with ice loss can differ

substantially from the global mean, due to gravitational, Earth deformational, and rotational effects (e.g. Clark & Lingle, 1977; Gomez et al., 2010; Mitrovica et al., 2001). Furthermore, past (ice age) ice cover changes lead to ongoing glacial isostatic adjustment (GIA) that contributes to regional variability in sea level rise. GIA effects can be considerable in regions such as in the Hudson Bay Complex (HBC, defined here as Hudson Bay, James Bay, Foxe Basin and Hudson Strait, Figure 6a) in Northern Canada that were once ice covered during the Last Glacial Maximum. In the HBC, sea level is presently falling due to GIA, but it is unclear if this trend will continue in the coming centuries due to the large uncertainties in the future evolution of the polar ice sheets, in particular the Antarctic Ice Sheet (e.g. Church et al., 2013; DeConto & Pollard, 2016; Golledge et al., 2015).

Here, we define sea level as the height of the sea surface relative to the solid Earth surface, or equivalently, ocean bathymetry. Global and regional patterns of sea level change have been shown to have a strong influence on ocean tides (e.g. Wilmes et al., 2017, Padman et al. 2018), because tides travel as shallow water waves, which are sensitive to ocean bathymetry. Changes in ocean bathymetry (caused by changes in sea surface height or ocean basin shape changes) can lead to changes in tidal wave propagation speed, energy dissipation, and amplitudes (Green, 2010). Variations in sea level and the associated changes in ocean tides can in turn affect other coastal processes and ecosystems such as the development of salt marshes, coastal erosion, frequency and magnitude of flood events, and saltwater intrusion of surface water (Craft et al., 2009; Kirwan & Guntenspergen, 2010; Kirwan et al., 2010; Kirwan & Megonigal, 2013; Nicholls & Cazenave, 2010; Ross et al., 2017). Finally, Arctic and sub-Arctic indigenous communities surrounding the HBC are among the most vulnerable to climate change (IPCC, 2014), with their livelihoods and food sources critically impacted by coastal changes (Lemmen et al., 2016; Tsuji et al., 2009, 2016).

Projections of future sea level change in the HBC due to climate change have been relatively limited. Gough (1998) suggested that sea level in Hudson Bay could begin to increase in the next century as the global mean sea level rise associated with climate change outpaces the sea level fall due to glacial isostatic uplift. However, Gough's simple model did not capture the spatial variability in sea level change that arises from melting current ice sheets. More recently, Tsuji et al. (2009, 2016) and Lemmen et al. (2016) calculated the spatially variable sea level change and suggested that glacial isostatic uplift would persist in parts of the HBC in the coming

centuries but did not consider a wide range of possible climate-driven sea level changes. Recent work has shown that even under the same climate forcing scenario, Representative Concentration Pathway (RCP) 8.5, projections of Antarctica's contribution to global mean sea level rise range from 2.25 m to 15.65 m by 2500 (DeConto & Pollard, 2016; Golledge et al., 2015, 2019). Given this large uncertainty, it is unclear what the dominant contributor to sea level change in the HBC will be, or even what the sign of sea level change will be. Furthermore, due to the relatively shallow bathymetry in the HBC, and the low-lying topography that surrounds the bay (Figure 6a), a small rise or fall in sea level will result in a large shoreline migration, amplifying the HBC's sensitivity to uncertainty in future sea level change.

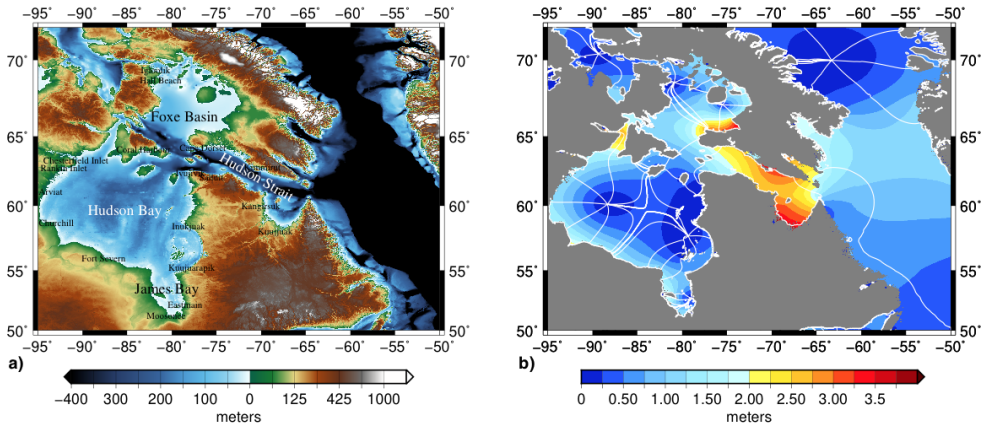

Figure 6: a) Bathymetry and topography of the Hudson Bay Complex, defined here as Hudson Bay, James Bay, Foxe Basin and Hudson Strait, b) Present day semi-diurnal (M_2) tidal amplitudes (colour) and phases (contoured in white lines at 1/8 M_2 period), taken from the TPXO8 tide database (http://volkov.oce.orst.edu/tides/tpxo8_atlas.html).

Previous regional studies have investigated future sea level and tide changes on the European Shelf (e.g., Idier et al., 2017; Pelling & Green, 2014; Pickering et al., 2012), the Patagonian Shelf (Carless et al., 2016), the Gulf of Maine (Pelling & Green, 2013), the Gulf of Mexico (Passeri et al., 2016), and the Bohai Sea in China (Pelling et al., 2013), but studies of the HBC are lacking. The HBC is a particularly interesting region with regards to ocean tides. The tidal range of Ungava Bay in Hudson Strait (16.8 m ± 0.2 m, Drinkwater, 1986), rivals that of the Bay of Fundy (17.0 m ± 0.2 m, O'Reilly et al., 2005), as the region with the largest tidal range in the world. Furthermore, Egbert & Ray (2001) found that more tidal energy is dissipated in the HBC alone than any other region in the world. This is because the HBC is near resonant at the

semi-diurnal tidal forcing frequency (Arbic et al., 2007; Webb, 2014), producing large semi-diurnal tides (exceeding 4 m amplitudes in some areas, Figure 6b) that are further amplified due to the HBC's location on a continental shelf (Clarke & Battisti, 1981). Due to the HBC being located on a shallow continental shelf, the HBC can strongly influence deep ocean tides in the connecting Atlantic Ocean (Arbic et al., 2009; Arbic & Garrett, 2010). Thus, any large-scale change in the HBC can have consequences far away from the region. Previous work on paleotides in the region indicated a strong sensitivity of ocean tides to changes in sea level (Arbic et al., 2004; Egbert et al., 2004; Uehara et al., 2006). However, modern tides in the HBC are not well resolved due to limited bathymetry data that can be used to constrain models (Egbert & Ray, 2001). Projecting future tides therefore requires, as a first step, an appraisal of the performance of available bathymetry models in reproducing modern tides in the HBC.

Wilmes et al. (2017) showed that a future complete collapse of the Greenland and West Antarctic ice sheets would strongly impact tides globally, and that simulations that take into account spatial variability in sea level change differ substantially from those that assume the global average equivalent rise. In particular, in Hudson Bay, the spatially variable sea level change associated with Greenland ice loss is opposite in sign to the uniform global average sea level rise scenario, which in turn results in large differences in predicted tidal changes. Furthermore, they show that spatially variable changes in sea level, and in turn tidal amplitudes in much of the HBC are positive under West Antarctic ice sheet collapse and negative under Greenland ice sheet collapse.

As a complete collapse of the Greenland and West Antarctic ice sheets represents a long term, upper bound on their contribution to sea level change, a question arises: How will future sea level and tides in the HBC evolve under combined, transient melting of the ice sheets in the coming centuries? A challenge in making multi-century, transient simulations is that there is a wide range of possibilities in the ice sheets', and in particular Antarctica's, contribution to future sea level change, primarily due to an incomplete description of physical processes and limited data to constrain ice-sheet model parameters (Kopp et al., 2017; Moore et al., 2013). To address this uncertainty, we consider a range of possible contributions to global sea level from the polar ice sheets and investigate the sensitivity of tides in the HBC to these changes. On decadal timescales, GIA will likely dominate, but on centennial timescales, the contribution from ice sheets could exceed GIA, in particular under high-end warming scenarios. This transition from a

regime of sea level fall to one of rise, and the associated changes in tides, is important to consider in assessing coastal climate change impacts and develop adaption strategies.

The present paper is structured as follows: In section 2.5, we describe the ice loss and sea level projections and the tidal model setup. Due to the sensitivity of tides to bathymetry, we discuss constraints on modern bathymetry in the HBC in section 2.6 and present a new bathymetry model that improves modern tide predictions. In section 2.7, we present predictions of future sea level changes associated with future retreat of the polar ice sheets and ongoing glacial isostatic adjustment and the associated tidal changes in the HBC. We conclude with a discussion in section 2.8.

2.5 Methods

2.5.1 Sea level and ice sheet modelling

We adopt the sea level theory from Kendall et al. (2005) and Gomez et al. (2010) to predict the spatially variable sea level changes resulting from past and future ice cover variations using a gravitationally self-consistent sea level model that incorporates viscoelastic deformation of the solid earth due to surface ice and ocean mass loading, migrating shorelines, and Earth rotational effects. Elastic and density structure of the solid Earth in all simulations is provided by the Preliminary Reference Earth Model (PREM) (Dziewonski & Anderson, 1981) and viscosity structure is given by the VM2 Earth model (Peltier, 2004) unless otherwise specified. The modern topography that serves as input to the sea level model is taken from GEBCO 2014 (Weatherall et al., 2015) globally, with the composite regional bathymetry described below over the HBC. All calculations are performed up to spherical harmonic degree 512.

We simulate the future evolution of the polar ice sheets in Greenland and Antarctica with dynamic ice sheet models. We focus on projections adopting RCP 8.5 (Collins et al., 2013), representing the business-as-usual emissions scenario as it serves as the upper bound of expected global temperature increase, and hence contribution of the ice sheets to sea level change in the HBC. Furthermore, by considering a single RCP scenario, we highlight the variability that emerges among ice loss and sea level projections that are guided by the same emissions framework.

Greenland and Antarctic ice thickness projections are generated using the Parallel Ice Sheet Model (PISM) version 0.7.3, a hybrid ice model with shallow shelf-shallow ice

approximations for floating and grounded ice (Winkelmann et al., 2011). Following the procedure outlined in Golledge et al. (2019), future climate forcing on the ice sheets is driven by the Coupled Model Inter-comparison Project Phase 5 (CMIP5) multi-model ensemble mean outputs. The ice sheet model simulations are performed on a high-resolution (2.5 km for Greenland and 5 km for Antarctica) polar stereographic grid. We apply a Gaussian smoothing filter on the changes in total (floating and grounded) ice thicknesses, then interpolate ice thickness predictions onto a lower resolution Gauss-Legendre 512 x 1024 global grid, to serve as input to the sea level model. We consider the Antarctic projection from Golledge et al. (2019) as the low-end projection of future Antarctic ice loss, hereafter referred to as the low-end scenario. We also consider an alternative simulation for the Antarctic Ice Sheet that predicts much greater ice loss. High-end projections of Antarctic ice thickness changes (hereafter referred to as the high-end scenario) are provided by a simulation in Pollard et al. (2017) using a coupled ice sheet – sea level model that includes ice cliff and hydrofracturing physics and a hybrid combination of shallow ice – shallow shelf approximations for ice dynamics. Ice thickness variations are provided by the ice model at 20 km resolution and then linearly interpolated onto the global 512 x 1024 grid.

To fully quantify the sea level changes in Hudson Bay, we also incorporate the contribution of ongoing GIA associated with past ice cover changes over the last deglaciation. We perform ice age sea level simulations adopting ICE-5G ice history with VM2 Earth model (Peltier, 2004) and ICE-6G with the VM5a Earth model (Argus et al., 2014; Peltier et al., 2015). Each simulation was run from 21ka to 500 years in the future, and the predictions of change from the modern (assumed here to be 2000 AD) to the year 2500 AD were added to the sea level changes associated with future ice sheet retreat described above (see Supplementary Figure S1 for a comparison of ICE-5G and ICE-6G).

The total sea level change is calculated as the sum of the contributions from Greenland, Antarctica, and GIA. Note that our projections do not include oceanographic effects. In the current century, these are expected to contribute a relatively uniform sea level rise in the bay under future climate warming (Jevrejeva et al., 2016), but the magnitude and timing of these changes is challenging to simulate in the HBC on multi-century timescales. While these effects would alter the timing of the change from a sea level fall to a sea level rise, they would likely not offset the overall effect of transitioning from a sea level fall to a sea level rise. In addition, the

size of the contribution is well within the range of Antarctic contributions considered here. Shorter timescale simulations should include the influence of ocean dynamics on sea level and tides.

2.5.2 Tide modelling

We use the Oregon State University Tidal Inversion Software (OTIS) (Egbert et al., 1994; 2004) to model present-day and future tides in Hudson Bay. OTIS solves the linearized shallow water equations forced by the tidal potential and with energy dissipation from bed friction and parametrised tidal conversion (e.g., Green & Nycander 2013; see Wilmes et al., 2017 for details on the model setup).

The HBC tide model was run at 1/30° x 1/30° horizontal resolution and simulated the tidal constituents M_2, S_2, and K_1. The extent of the model domain is shown in Figure 6. Dissipation of tidal energy was calculated according to Egbert & Ray (2001; see also Wilmes et al., 2017 for a detailed description). For the present-day simulations, TPXO8 (Egbert & Erofeeva, 2002; see http://volkov.oce.orst.edu/tides/tpxo8_atlas.html for the latest version) elevations were used as forcing at the open boundaries. TPXO8 is an observation constrained model solution which assimilates tide gauge observations and satellite altimetry to produce a highly accurate estimate of the tides (~2 cm RMS error compared to un-assimilated tide gauge data; see Egbert & Erofeeva, 2002, and Stammer et al., 2014, for details).

For the future tide simulations, sea level change predictions described in section 2.1 are added to the present-day bathymetries for both HBC and the global setup. Simulations are performed for 2100, 2300, and 2500 AD. Elevation changes in response to the future sea level changes simulated by a near-global 1/8° x 1/8° (86° S - 89° N) tidal model were added to the boundary conditions used for the present-day simulations, thereby ensuring a high degree of accuracy for high-resolution HBC future simulations.

2.6 Constraints on modern bathymetry

Numerical prediction of tides in near-resonant basins, such as Hudson Bay, are strongly sensitive to the adopted ocean bathymetry (Egbert & Ray, 2001; Green, 2010; Padman et al. 2018). Therefore, in order to project future tide changes, we require an accurate estimate of modern bathymetry. Bathymetry in the HBC is poorly constrained due to the sparsity of available data, related to the HBC's shallow depths, spatial extent, and limited commercial

shipping routes. Furthermore, there is substantial disagreement between global bathymetry datasets in the HBC (Supplementary Figure S2); differences between datasets reach up to 200 m in some areas of the complex. As a result, tide models struggle to accurately capture the tides in the region.

Given the lack of available data to distinguish between these bathymetry models, we seek to simultaneously find a bathymetry to use for (future) projections and to improve modelling of the modern tide. To do this, we simulate modern tides in the HBC using the configuration described in 2.2 with a suite of different bathymetry models GEBCO 2008 (see The GEBCO_2008 Grid, version 20100927, www.gebco.net), GEBCO 2014 (Weatherall et al., 2015), ETOPO1 (Amante & Eakins, 2009), and SRTM30_Plus (Becker et al., 2009) and compare the simulated tidal amplitudes to the observed tides in TPXO8.

Figure 7a-c show the difference between the simulated M_2 tidal amplitudes using three of the four bathymetry datasets considered (GEBCO 2008, GEBCO 2014, and SRTM30_Plus) and the TPXO8 observations. We also calculate the root mean square error (RMSEs) against TPXO8 to evaluate the performance of bathymetry models in reproducing modern tides over the global domain, see also Table 1 for a quantification of the errors. RMSEs are shown for all ocean depths (total RMSE) and deep oceans regions (water depths > 500 m, deep RMSE).

The simulation using ETOPO1 (Amante & Eakins, 2009) (not shown) produced the largest errors of all the simulations, differing from observations by more than 1 m in Hudson Strait and James Bay. Both GEBCO 2014 (Figure 7a) and GEBCO 2008 (Figure 7c) perform well in Hudson Strait, each with basin RMSEs of 15 cm and 21 cm, respectively. In Hudson Bay, SRTM30_Plus (Figure 7b) matches more closely than the GEBCO simulations, differing from TPX08 with a basin RMSE of 7 cm. The largest amplitude errors in all simulations are in Hudson Strait, where there are also the largest differences in depths between datasets (Supplementary Figure S2) and the largest tidal amplitudes (Figure 6b).

In an attempt to improve the accuracy of the tidal simulations, we develop a new, composite bathymetry (Figure 7d) based on how well each existing bathymetry dataset performed regionally in the comparison to TPXO8 in the HBC. Our composite bathymetry merges, using linear weighting, SRTM30_Plus bathymetry in Hudson Bay and GEBCO 2008 bathymetry elsewhere in the HBC. The modern tide simulation adopting the composite bathymetry differs from TPX08 in Hudson Bay with a basin RMSE 6 cm. The largest amplitude

errors in James Bay and Foxe Basin are less than ± 25 cm, with basin RMSEs of 5 cm and 13 cm, respectively. Our composite bathymetry improves the amplitude fit in Hudson Strait, with amplitude RMSE of 20 cm when compared to TPXO8. Furthermore, we find that our composite, regional bathymetry substantially reduces both total and deep RMSE (Table 1), compared to the global bathymetry models (Table 1). Consequently, we adopt this composite, modern bathymetry in the future sea level and tide projections shown in the sections to follow.

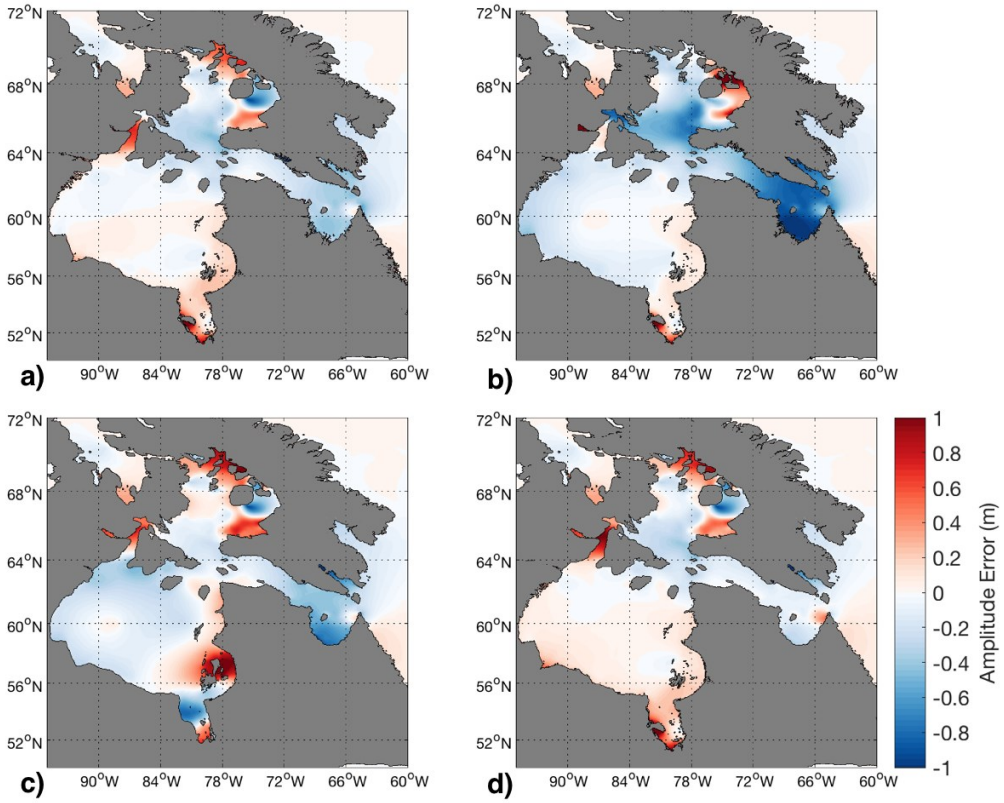

Figure 7: Amplitude error between simulated M_2 amplitudes from several bathymetry datasets and observed M_2 amplitudes from TPXO8. a) GEBCO 2014 (Weatherall et al., 2015), b) SRTM30_Plus (Becker et al., 2009), c) GEBCO 2008 (http://www.gebco.net), d) our new, composite bathymetry with SRTM30_Plus in Hudson Bay and GEBCO 2008 elsewhere.

	M_2 amplitude Root Mean Square Error (RMSE)	
	Total RMSE (cm)	**Deep ocean (>500 m) RMSE (cm)**
ETOPO1	25.8	7.3
GEBCO 2008	19.4	4.1
GEBCO 2014	20.8	4.5
SRTM30_Plus	22.9	7.3
Composite bathymetry	14.2	3.4

Table 1: Total (all water depths) and deep ocean (water depths > 500 m) root mean square error between predicted M_2 amplitudes from several bathymetry datasets and observed M_2 amplitudes from TPXO8.

2.7 Results

2.7.1 Sea level change

Figure 8 shows the projected contributions to sea level change in the HBC associated with GIA and melting from the Greenland Ice Sheet and Antarctic Ice Sheet for the three time slices 2100, 2300 and 2500 (see Supplementary Figure S4 for the total sea level change adopting ICE-6G). The contribution from GIA (Figure 8a-c) shows a sea level fall across the HBC. The regions of maximum predicted sea level fall are James Bay and Churchill, Manitoba (see Figure 6a for the location of these regions) where the magnitude of sea level fall is 1.2 m, by 2100 and 5.9 m and 5.7 m respectively, by 2500. Foxe Basin experiences a maximum sea level fall associated with GIA of 0.9 m by 2100 and 4.3 m by 2500. This is driven by the larger thickness of the Laurentide Ice Sheet during the Last Glacial Maximum in these regions and the later termination of deglaciation. Hudson Strait sees a more moderate fall of 0.3 m by 2100 and 1.5 m by 2500. In contrast, to the east of the HBC in Davis Strait region, sea level rises over the 500-year GIA simulation (red regions in Figure 8a-c) due to the subsidence of peripheral bulges that formed around the ice sheets at the Last Glacial Maximum in our ICE-5G simulation.

Next, we consider the contribution from melting of the polar ice sheets (Figure 8d-l). There are a number of physical effects contributing to the differences in sea level change in the HBC associated with Greenland (Figure 8d-f) and Antarctic ice loss (Figure 8g-l). An ice sheet exerts a gravitational attraction on the surrounding water, and this attraction weakens as the ice sheet loses mass, resulting in a local sea level fall within ~2000 km of the ice loss (Woodward, 1888). At greater distances from the source of ice loss, sea level rises more the global average (Tamisiea & Mitrovica, 2011). Uplift of the solid Earth in and around the region of ice loss further accentuates the local sea level fall, and deformation of the Earth due to loading of the oceans with water and changes in the planet's rotation associated with surface mass redistribution add geographic variability to the sea level change farther away from the ice sheet. In our simulations, the Greenland ice sheet is projected to contribute 0.10 m and 0.55 m of global averaged sea level rise by 2100 and 2500, respectively, but the HBC is within the zone of gravity-driven sea level fall for the Greenland ice sheet. Therefore, Greenland melting is projected to contribute a low amplitude drop in sea level across the HBC that decreases in amplitude with distance from Greenland. The smallest sea level decrease occurs in the south-eastern part of the HBC (Figure 8d-f and Supplementary Figure S3a) and the largest sea level fall can be seen in northern Foxe Basin (up to 0.7 m by 2500) and the northern Labrador Sea. In Hudson Strait, the projected sea level decrease reaches 0.5 m by 2500. Central Hudson Bay would experience up to a 0.2 m decrease in sea level by 2500. In James Bay, sea level remains unaltered by 2100, with a shift to a sea level rise by 2500 that does not exceed 0.10 m. The sea level fall due to Greenland melting is an order of magnitude smaller than that caused by GIA. Sea level in the HBC is hence relatively insensitive to Greenland ice loss due to the fingerprint pattern and the proximity of the southern and western coasts of the HBC to the region net-zero sea level change.

Melting from the Antarctic ice sheet, on the other hand, would lead to a sea level rise in the HBC that is approximately 1.2 times greater than the global mean sea level equivalent rise associated with the melting, with a relatively uniform rise across the HBC (Supplementary Figure S3b). Figure 8g-l shows the projected sea level changes in response to the low-end (Figure 8g-i) and high-end (Figure 8j-l) Antarctic ice loss scenarios under RCP8.5. Under the low-end simulation, Antarctic melting would lead to a maximum sea level rise in the HBC of 0.1 m by 2100 and 2.1 m by 2500. The high-end scenario (j-l) predicts an order of magnitude larger

sea level rise of up to 0.8 m across the HBC by 2100. By 2500, the high-end simulation predicts a sea level rise of around 14.5 m.

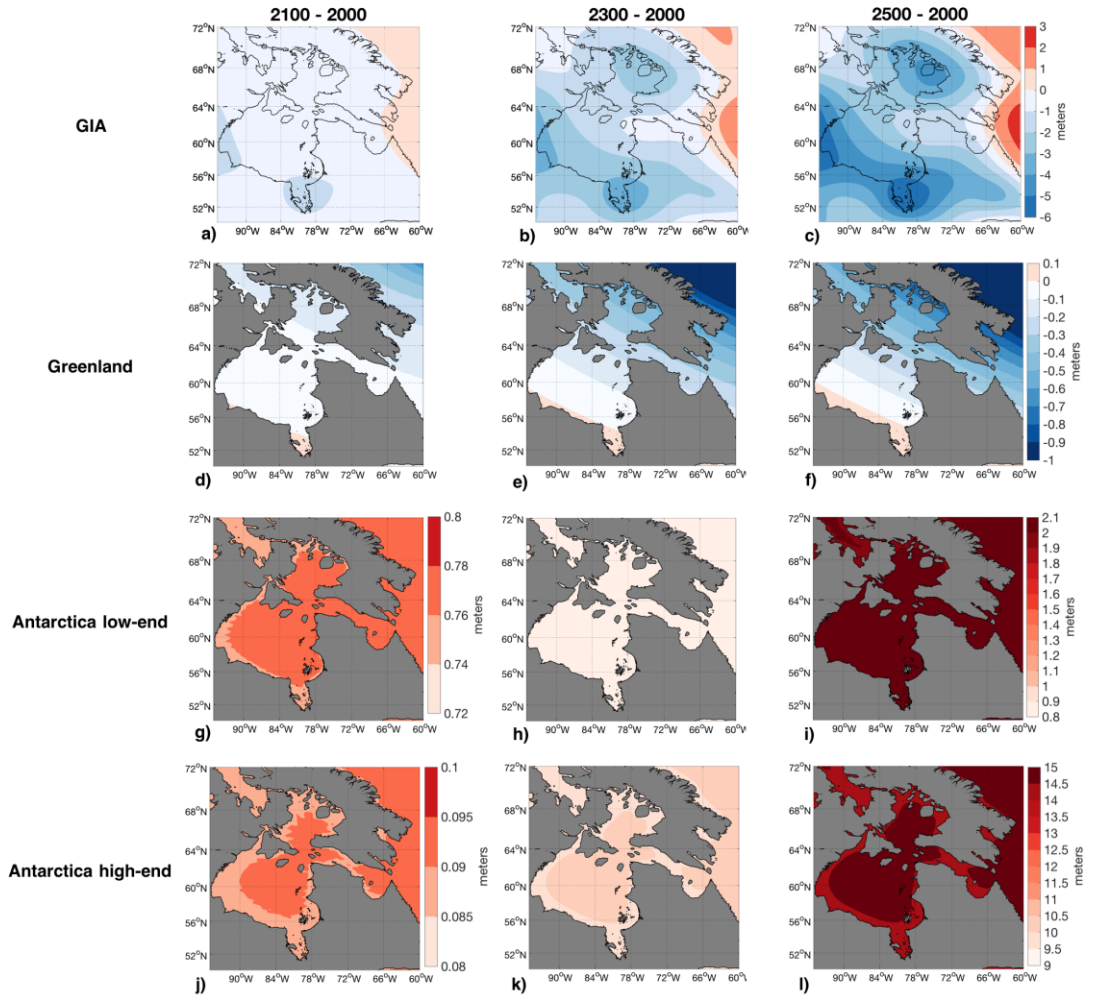

Figure 8: Contributions to sea level change in the HBC from GIA and future melting of the polar ice sheets under RCP8.5 at 2100, 2300 and 2500, relative to 2000. Blue shading corresponds to a sea level fall and red shading corresponds to a sea level rise. (a-c) Contribution to sea level change from past ice-ocean loading changes (i.e. GIA) over the last deglaciation associated with the ICE-5G ice history (Peltier, 2004). (d-f) Contribution to sea level change from the Greenland Ice Sheet (Golledge et al., 2019. (g-l) Contribution to sea level change from the Antarctic Ice Sheet under from (g-i) low-end (Golledge et al., 2019) and (j-l) high-end (Pollard et al., 2017) projections. Note the different color scales used for the 2100, and the 2300 and 2500 projections in panels g-l.

In Figure 9, we consider the sum of all the contributions shown in Figure 8 (see also Supplementary Figure S4 for the total sea level change adopting ICE-6G). Under the low-end Antarctic ice loss scenario (Figure 9a-c), the sea level change at 2100, 2300, and 2500 is dominated by GIA effects. The largest sea level decreases are predicted in the regions where the signal from GIA is greatest (Figure 8a-c). At 2100 (Figure 9a), the magnitude of sea level fall ranges from 1.1 m in Churchill to 1.2 m in James Bay. In Hudson Strait, the amplitude of sea level fall is damped and on the order of 0.4 m. East of Hudson Strait in the Davis Strait, a slight rise is seen, where Antarctic ice loss and GIA are both contributing a sea level rise. By 2300 (Figure 9c), the sea level fall ranges from 1 m in central Hudson Bay up to 2.75 m in James Bay. Ungava Bay, at the entrance of Hudson Strait, is the only area in the HBC that experiences a sea level rise, reaching up to 0.4 m. Thus, despite that the largest sea level fall due to GIA and Greenland ice loss is predicted for the Hudson Strait (Figure 8d-f), the sea level rise associated with Antarctic ice loss still dominates the sea level change. By 2500, the sea level fall across much of the HBC reaches 3 m. Our low-end simulation suggests a gradual extension of sea level rise into the HBC. By 2500, the extent of sea level rise spreads westwards from the Hudson Strait into Hudson Bay, where sea level rise is less than 0.50 m.

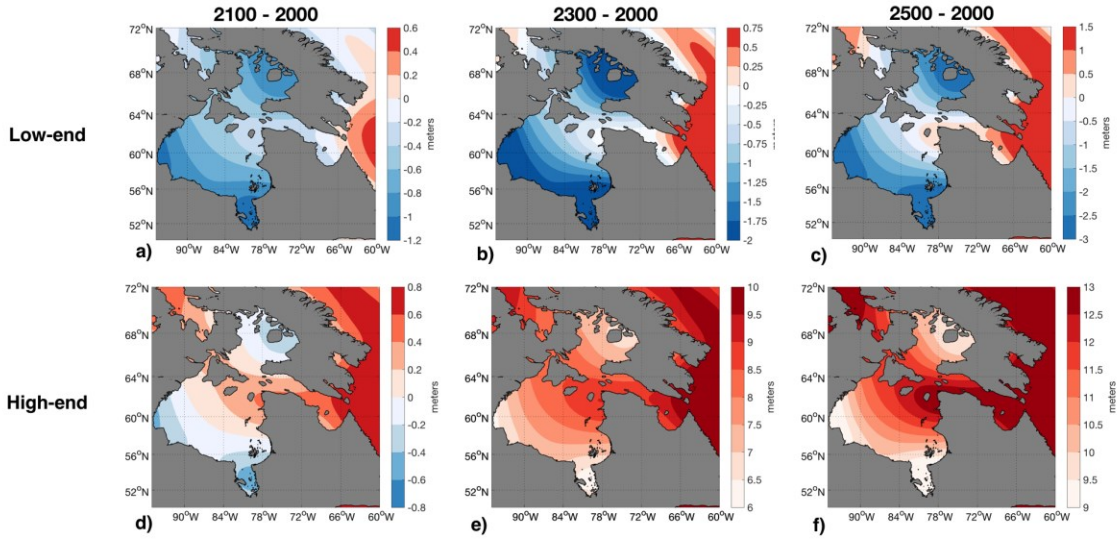

Figure 9: Total projected sea level change at 2100, 2300, and 2500, relative to 2000. Sum of individual contributions presented in **Figure 8**. Panels a-c correspond to the low-end Antarctic ice loss scenario (Golledge et al., 2019). Panels d-f correspond to the high-end Antarctic ice loss scenario (Pollard et al., 2017).

The projection that incorporates the high-end Antarctic scenario is characterized by a transition from sea level fall to sea level rise across the HBC over the simulation time. At 2100 under this high-end Antarctic scenario (Figure 9d), GIA still dominates in Hudson Bay, James Bay and northern Foxe Basin. In other regions of the HBC, the signal of sea level rise from Antarctic ice loss already begins to outpace the signal from GIA. We find that by 2200 (Supplementary Figure S5) sea level has begun to rise across the entire HBC. Despite the large GIA signal in Foxe Basin and James Bay, our projections indicate that these regions would experience up to 3 m of sea level rise by 2200 and that sea level rise in other regions in the HBC reaches up to 4.5 m. In 2300 (Figure 9e), a maximum sea level rise of 9.5 m is predicted in Ungava Bay in Hudson Strait, with the smallest rise of 6.3 m in James Bay. The magnitude of minimum sea level rise under the high-end scenario at 2300 is triple the magnitude of maximum sea level fall predicted from the low-end scenario. At 2500 (Figure 9f), sea level rise exceeds 14 m in some regions of Hudson Strait. In Foxe Basin, the projected 10 m rise by 2500 represents, on average, a 10% increase in water depth, relative to present day. Moreover, the 9 m rise predicted for James Bay suggests a 20% increase in water depth relative to present day. As in 2300, we find that the magnitude of minimum sea level rise in James Bay and Foxe Basin under the high-end scenario in 2500 is three times the magnitude of maximum sea level fall calculated from the low-end scenario.

2.7.2 Tides

In Figure 10, we present the M_2 tidal amplitude changes associated with the total sea level changes presented in Figure 9. The tidal M_2 amplitude responses differ substantially between the low-end (Figure 10a-c) and high-end (Figure 10d-e) scenarios.

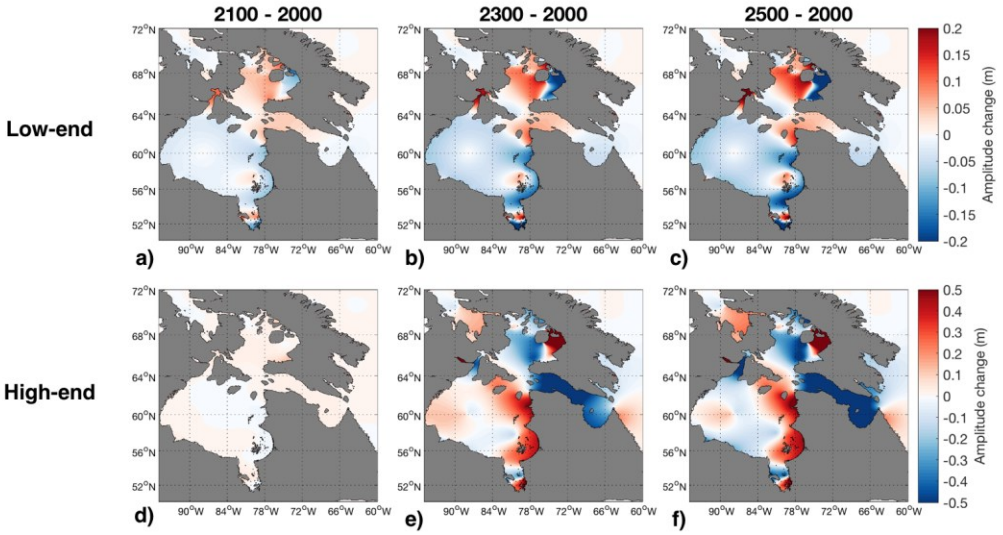

Figure 10: Total projected M_2 amplitude change at 2100, 2300, and 2500, relative to 2000. Panels a-c correspond to tidal changes associated with the low-end Antarctic ice loss scenario (Golledge et al., 2019). Panels d-f correspond to tidal changes associated with the high-end Antarctic ice loss scenario (Pollard et al., 2017).

For the low-end scenarios, all time slices show the same pattern of M_2 tidal amplitude response that increases in magnitude over time, reaching a maximum of -0.2 to +0.2 m by 2500. Hudson Bay is dominated by a decrease in M_2 tidal amplitude. These changes are associated with the northeastward shift of the eastern amphidrome (point of zero-amplitude tide, indicated by the intersection points of the co-tidal phase lines in Figure 6b). Tidal amplitudes increase in the north-east part of the bay, central James Bay and Roes Welcome Sound in northwestern Hudson Bay. At the entrance to Hudson Strait and Ungava Bay small decreases in amplitudes can be seen, however, in none of the time slices do the changes exceed 5 cm. At the western end of Hudson Strait, small tidal amplitude increases can be seen (< 10 %). In Foxe Basin, the eastern amphidrome shifts eastward and the western one moves to the north west, leading to tidal amplitude increases in the central and western parts of the bay (up to 20 cm for 2500). Also, in the easternmost part of the basin, tidal amplitudes decrease because of the amphidromic motions.

The responses for the high-end scenarios for 2300 and 2500 in most locations are of opposite sign to the ones seen in the low-end scenarios and are generally of much larger magnitude. For the 2100 projections the tidal amplitude changes do not exceed 3 % and will

therefore not be discussed. In the high-end 2300 and 2500 scenarios, strong tidal amplitude decreases can be seen for Hudson Strait and Ungava Bay exceeding 60 cm for 2300 and 1 m for 2500 and translating to a drop in tidal amplitudes of around 30 % in large parts of the strait. In Hudson Bay, tidal amplitudes in the 2300 scenario generally increase whereas for the 2500 case they occur mainly in the eastern half of the bay. Here, amplitude increases exceed 300 % in some locations corresponding to a > 60 cm increase. The amplitude increases are associated with the eastward shift of the western amphidrome and the eastward shift of the western amphidrome. In James Bay, the amphidrome shifts northward resulting in increased amplitudes in the southern part of the bay and decreases in the north. Foxe Basin is dominated by amplitude decreases in the central and eastern part of the basin, but large amplitude increases of more than 1.8 m for the 2500 projection can be seen along the eastern margins of the bay. These increases are linked to a westward shift of the amphidrome located close to Prince Charles Island.

Integrated dissipation in the HBC for all the low-end scenarios time slices and at 2100 for the high-end scenario remains at the present-day level of 230 GW. At 2300 and 2500 under the high-end scenario, integrated dissipation drops to 170 GW and 149 GW. This represents decreases of 26 and 35 %, respectively, which, given that HBC at present is one of the regions on the globe where most energy is lost from the tide, could affect the global tidal energy budget.

2.8 Discussion and Conclusions

We have modeled future sea level changes in the Hudson Bay associated with ice loss from the Greenland and Antarctic ice sheets and GIA and their impact on ocean tides in the region. We showed that both sea level and tides in the HBC are relatively insensitive to Greenland melting (Supplementary Figure S6) but strongly sensitive to Antarctic ice sheet evolution, with our simulations indicating a transition from a sea level fall to a sea level rise across the HBC that is dependent on the adopted Antarctic ice loss scenario. In this work, we focused on the RCP8.5 emissions pathway, however more moderate warming scenarios such as RCP2.6 or RCP4.5 could prolong the time period of sea level fall in the HBC.

Our results indicate that the sea level fall associated with GIA contributes significantly to sea level change in the HBC and dominates under low-end Antarctic ice loss scenarios. HBC is dominated by sea level decreases (up to 1.2 and 3 m by 2100 and 2500, respectively). Hudson Strait is the only region that experiences sea level rise (up to 0.5 m by 2500). We found that the

associated M_2 tidal amplitude changes are less than 0.20 m in the HBC by 2500, with tidal amplitude increases in Foxe Basin and western Hudson Strait, and tidal amplitude decreases across Hudson Bay, James Bay, and Ungava Bay in Hudson Strait. We have shown that small migrations of the amphidromic points are responsible for the observed changes in the M_2 tides.

Conversely, GIA does not compensate the projected sea level rise under more rapid Antarctic ice loss in our high-end scenario. In the projection adopting the high-end Antarctic ice loss scenario, sea levels begin to rise in much of the HBC by 2100, with a widespread transition from sea level fall to sea level rise by 2200 and reaching a peak sea level rise of 14 m in Ungava Bay in Hudson Strait by 2500. Under the high-end scenario, the M_2 tidal amplitude changes reach up to 1 m with the largest decreases occurring in Hudson Strait and Foxe Basin and peak increases along the eastern margin of Hudson Bay by 2500. Furthermore, as the Hudson Bay Complex is presently one of the areas on the planet where the most tidal energy is dissipated (Egbert & Ray, 2001) the significant changes in dissipation (>150% in eastern HBC, see Supplementary Figure S8d-f) suggested under our high-end scenario simulations could affect the global tidal energy balance.

We find the strongest sensitivity of ocean tides to sea level changes in Hudson Strait, where the basin is close to resonance for the M_2 tidal period (e.g. Arbic et al., 2009; Webb, 2014). Our Hudson Strait results under the high-end scenario are in agreement with Arbic et al. (2007). They suggested that an increase in sea level by 7 m would shift the resonance period of Hudson Strait from 12.7 h to 12.4 h, bringing it to equal the M_2 tidal period, whereas sea level changes exceeding 7 m could shift the system further away from resonance and decrease tidal amplitudes (see our Figure 10d-f) and tidal dissipation (see our Supplementary Figure S7d-f). Repeating the resonance calculations by assuming a mean water depth of 154 m and a basin length of 890 km shows that sea level increases of 10 m and 13 m as seen for the 2300 and 2500 high-end scenarios would further decrease the natural period to 12.3 h and 12.2 h, respectively, thus agreeing with our modelled decreases in tidal amplitudes and dissipation. However, an additional simulation conducted for the year 2200 with the high-end Antarctic ice loss scenario, in which sea-level increases of 4 – 5 m occur in Hudson Strait, shows decreases in amplitude across Hudson Strait similar to the 2300 and 2500 simulations (see Supplementary Figure S5). This, in contrary to Arbic et al. (2007), suggests that Hudson Strait might be closer to resonance at M_2 frequencies at present than previously assumed, and even small decreases in sea-level

decrease the strait's resonance period, therefore leading to decreases in M_2 amplitudes and dissipation.

Our HBC tidal responses are in good agreement with the results from the global simulations shown in Wilmes et al. (2017). They compared tidal amplitude responses to non-uniform sea level changes due to full collapses of the West Antarctic Ice Sheet and the Greenland Ice Sheet and a uniform sea level rise of 12 m. The spatially variable sea level change scenario had a similar magnitude sea level fall over the HBC as the 2500 low-end scenario whereas the uniform sea level rise case was most akin to the 2500 high-end case shown here. The amplitude responses to the two different scenarios agree in their patterns between the two studies which gives us confidence in the results presented here.

Here, we focused on the contributions due to ice mass loss from the polar ice sheets and GIA associated with the last deglaciation, however, melting of mountain glaciers, oceanographic and sea ice changes in the HBC will also impact sea level and ocean tides, in particular on timescales shorter than the centennial timescales considered here. By 2100, melting from mountain glaciers under RCP8.5 is expected to contribute on the order of 0.2 m of sea level fall across the HBC (Jevrejeva et al., 2016), equal in magnitude but opposite in sign to the globally averaged value (Church et al., 2013). By 2500, the globally averaged sea level rise from mountain glaciers is projected to be between 0.30 – 0.40 m (Church et al., 2013). Conversely, thermal expansion and ocean dynamics are expected to contribute on the order of 0.3 m of sea level rise in the HBC under RCP8.5 by 2100 (Jevrejeva et al., 2016), similar to the contribution of these effects to globally averaged sea level rise of 0.21-0.33 m by 2100 estimated in the IPCC (Church et al., 2013). While regional estimates in the HBC are limited on multi-century timescales, the contribution of thermal expansion and ocean dynamics to globally averaged sea level rise under RCP8.5 is estimated to be between 0.29-1.81 m by 2300, and 0.37-2.77 m by 2500 (Church et al., 2013). In the HBC in the current century, the sea level fall associated with the loss of mountain glaciers could offset the sea level rise associated with Antarctic ice loss. On multi-century timescales, the contribution of these effects is less certain and may impact the timing of the transition from sea level fall to sea level rise. Incorporating projections of changes in ocean dynamics and mountain glaciers would improve projections of sea level and tide changes in the HBC. Furthermore, we have considered changes in sea level and tides in the HBC during the ice-free season. Since Hudson Bay is currently characterized by a long sea ice cover

season which dampens the magnitude of the tides (Godin, 1986; Kleptsova & Pietrzak, 2018; St-Laurent et al., 2008), future work will explore the impact of retreating sea ice on our results.

Previous simulations of modern tides have had large amplitude errors in the HBC (e.g., Wilmes et al., 2017) due to large uncertainty in the bathymetry in the HBC. We have developed a new method for constraining bathymetry using tide observations that greatly improves the fit between predicted and observed modern tides, with total, and deep ocean root mean square errors less than 15 and 4 cm, respectively. Our methodology may be used to further refine bathymetry models in the Hudson Bay Complex and in other regions with sparse data. Our results also highlight the need for high-resolution bathymetry surveys in the HBC, a region that will become increasingly important as sea ice cover retreats and access via marine traffic increases in a warming climate. Furthermore, accurate bathymetry data has far-reaching implications for residents surrounding the HBC, including, for example, future land claim issues related to the formation of land bridges between islands and the mainland (Tsuji et al., 2016).

We emphasize that results from this research have profound impacts on ecosystems and communities surrounding the HBC. Due to the shallow topography and bathymetry in the HBC, we project that an increase in the absolute depth of water of up to 20% could occur by 2500 under our high-end scenario, which would lead to changes in the extent of the intertidal zone and shoreline locations, in turn affecting ecosystems including wetlands and marshes. If sea level rise outpaces the rate at which marshes grow, these areas will become inundated, reducing the capacity of these ecosystems to attenuate storm surges and flooding events (Kirwan & Guntenspergen, 2010). Furthermore, the livelihoods, culture, and traditions of indigenous communities surrounding the HBC are strongly linked to the natural environment. Coastal management and policy decisions should integrate the physical changes presented here. In doing so, these vulnerable groups will be better equipped to deal with future impacts of climate change on coastal regions.

We conclude that projections of changes in sea level and ocean tides in the HBC should take into account not only the sea level changes due to ongoing glacial isostatic adjustment from the past deglaciation, but also consider a range of spatially variable sea level change projections arising from land ice loss, in particular in Antarctica. Uncertainty in projections of change in coastal areas in the HBC is dominated by uncertainty in projections of the evolution of the

Antarctic ice sheet. As our understanding of the response of Antarctica to climate change improves, so too will our projections of sea level and tide changes in the Arctic.

2.9 Supplementary Figures

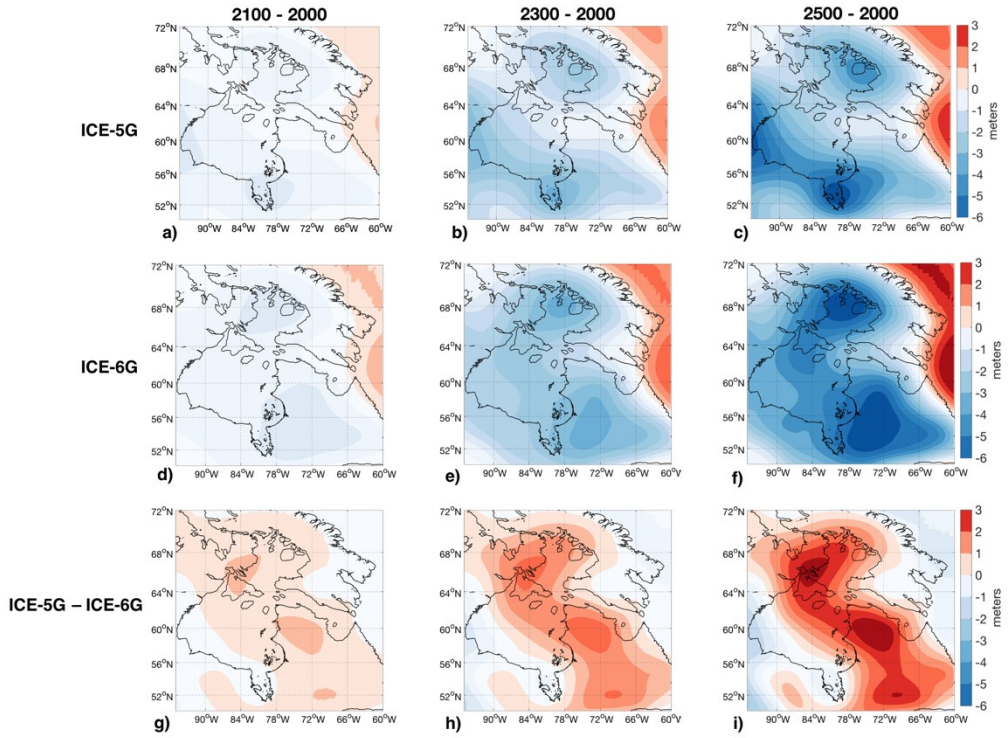

Figure S1: Contribution of glacial isostatic adjustment (GIA) to sea level changes in the Hudson Bay Complex at 2100, 2300, and 2500 relative to 2000 adopting ICE-5G (Peltier, 2004) (a-c) and ICE-6G (Argus et al., 2014; Peltier et al., 2015) (d-f) ice histories. Panels g-i represent the difference between panels a-c and d-f. Note that in the main manuscript, we adopt the ICE-5G ice history as the spatial pattern of ice loading and unloading in ICE-6G in this region is unrealistic.

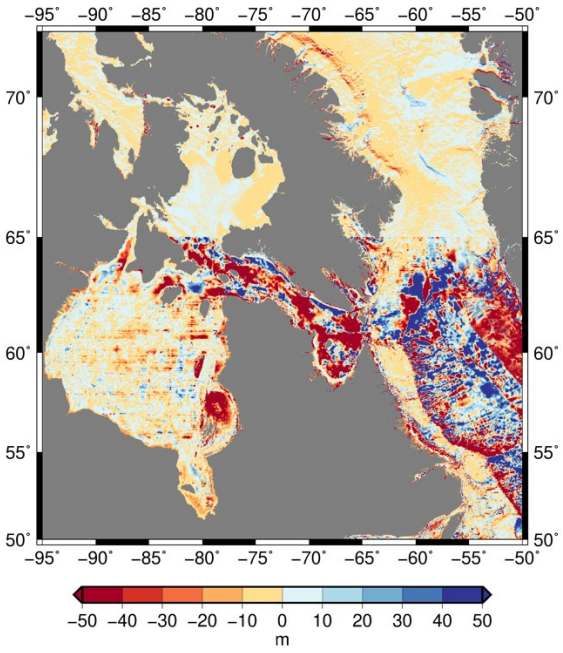

Figure S2: Difference between the GEBCO 2014 and ETOPO bathymetry datasets. Differences are saturated beyond ± 50 meters, but exceed 200 meters in parts of Hudson Strait.

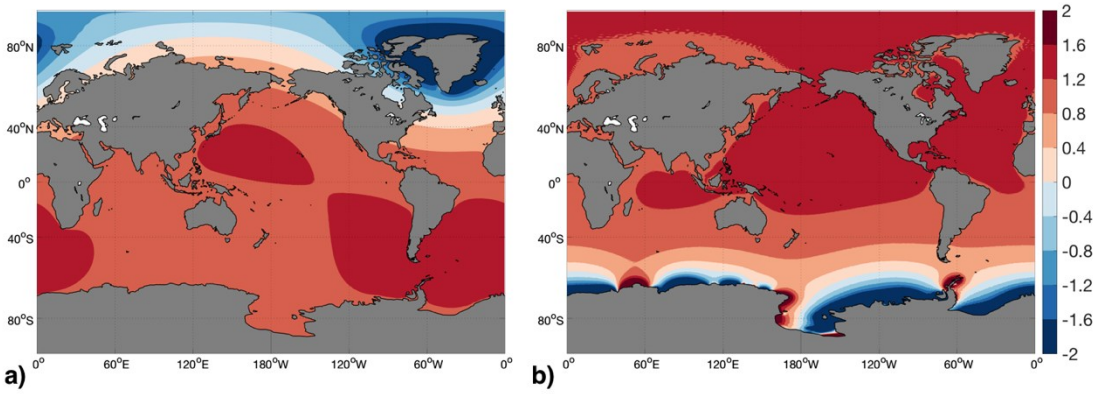

Figure S3: Normalized fingerprint of sea level change associated with melting of a) the Greenland Ice Sheet and b) the Antarctic Ice Sheet. Normalized fingerprints are calculated by dividing the spatially variable sea level change by the eustatic equivalent value (EEV, or global average) of sea level change associated with the ice loss.

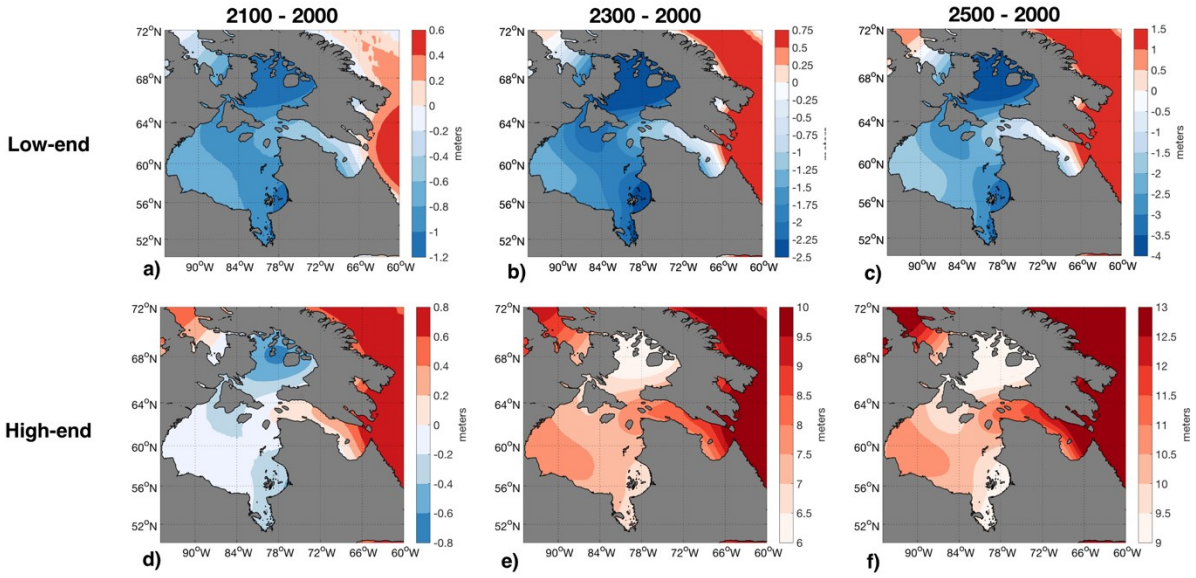

Figure S4: Total projected sea level change at 2100, 2300, and 2500, relative to 2000, adopting the ICE6-G ice history (Argus et al., 2014; Peltier et al., 2015). Sum of individual contributions presented in **Figure 8**. Panels a-c correspond to the low-end Antarctic ice loss scenario (Golledge et al., 2019). Panels d-f correspond to the high-end Antarctic ice loss scenario (Pollard et al., 2017).

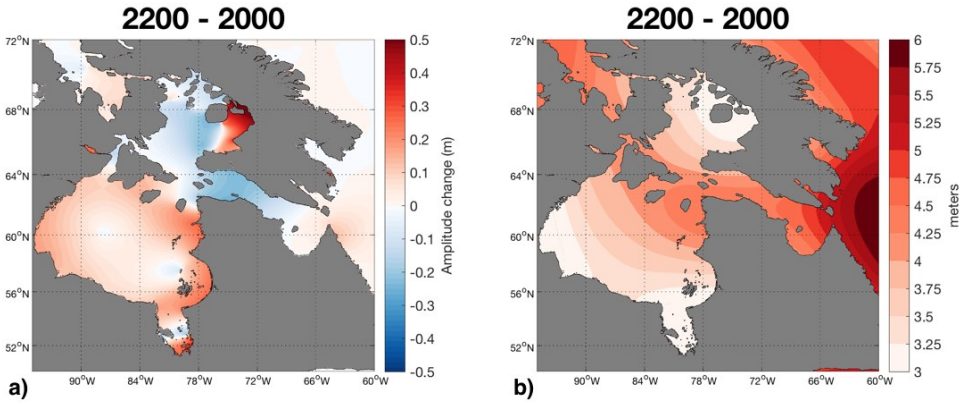

Figure S5: Total projected a) sea level and b) tidal amplitude changes at 2200, relative to 2000, incorporating the contributions of Greenland ice loss, GIA, and the high-end Antarctic ice loss scenario.

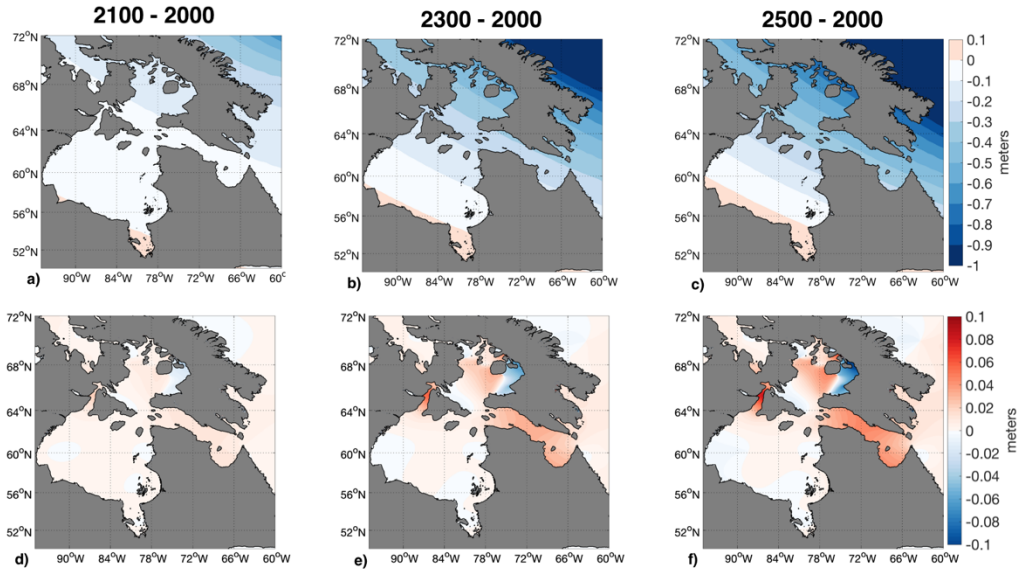

Figure S6: Sea level (a-c) and M_2 tidal amplitude (d-f) changes associated with Greenland ice loss at 2100, 2300 and 2500, relative to 2000.

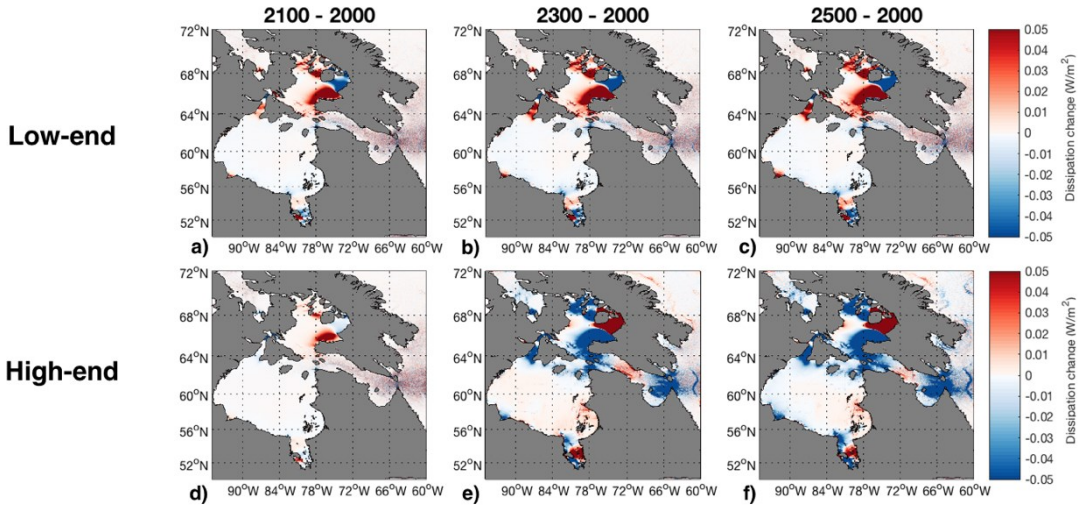

Figure S7: M_2 tidal energy dissipation change at 2100, 2300, and 2500, relative to 2000 under our low-end (a-c) and high-end (d-f) Antarctic ice loss scenarios.

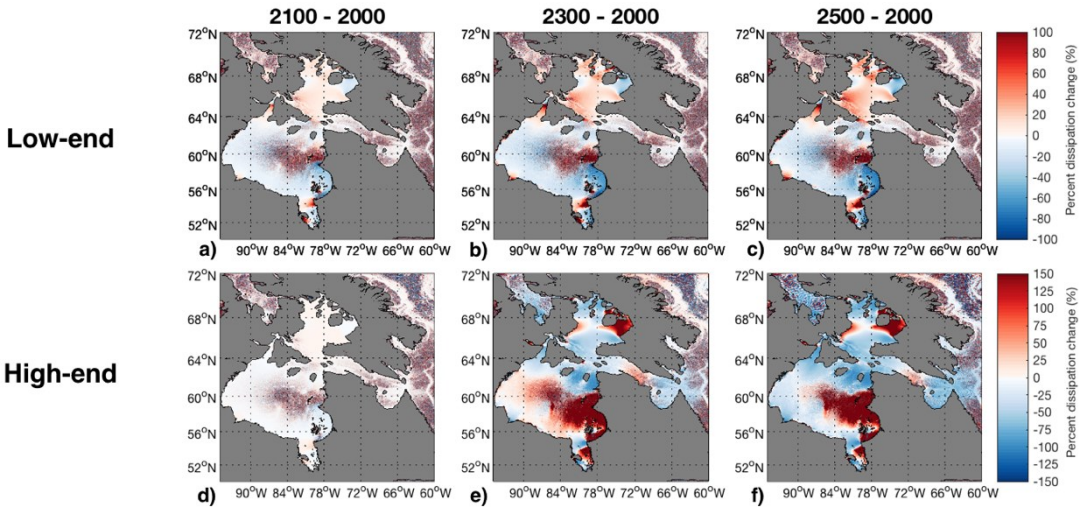

Figure S8: Percent M_2 tidal energy dissipation change at 2100, 2300, and 2500, relative to 2000 under our low-end (a-c) and high-end (d-f) Antarctic ice loss scenarios.

3. Conclusions and Implications of research

3.1 Conclusions

The aim of this thesis was to investigate the future evolution of sea level and tides in Hudson Bay in response to climatically driven changes in past and future ice sheets. This objective was achieved according to the results presented in Chapter 2.

It was found that sea level and tides in Hudson Bay are relatively insensitive to Greenland ice loss, but highly sensitive to Antarctic ice loss. It was shown that under low-end Antarctic ice loss, the contribution of glacial isostatic uplift would dominate the sea level change signal, prolonging the sea level fall in the region for the next 500 years. Across most of the region, the associated tidal amplitude changes were small (< 0.20 m) decreases. Conversely, under the high-end Antarctic ice loss scenario, it was found that there would be a transition from a regime of sea level fall to one of rise by 2200 in Hudson Bay. By 2500, the high-end scenario indicated that sea level would rise up to 14 m. Projected changes in tidal amplitudes were in most locations opposite in sign from those in the low-end scenario, in addition to being much larger (up to 0.50 m). Under the low-end scenario, future integrated tidal dissipation would remain at present day levels of 230 GW, whereas under the high-end scenario, integrated tidal energy dissipation would decrease by 35% by 2500. Tidal amplitudes in the adjacent Hudson Strait showed the strongest response in both low- and high-end scenarios, with the strait moving away from tidal resonance for the M_2 period under the high-end scenario.

3.2 Future research directions

While this work focused on future sea level and tide changes on centennial timescales, future avenues of research could consider other timescales and time periods. For example, we are in the process of modeling sea level and tide changes in the Hudson Bay following retreat of the Laurentide Ice Sheet across the Hudson Bay Complex during the Last Deglaciation. Future work could also focus on decadal-timescale projections, where on these timescales, the effects of ocean thermal expansion on future sea levels and tides would also need to be considered. As indicated in Chapter 2, thermal expansion is expected to contribute a relatively uniform sea level rise of 0.3 m across the bay by 2100 (Jevrejeva et al., 2016), which could alter the timing of the transition from a regime of sea level fall to one of rise.

In addition to sea level changes, there are other processes that could impact future tides in the region. The results presented in Chapter 2 did not account for sea ice cover in Hudson Bay, which currently persists in the bay from October-July. The presence of sea ice modifies the timing of low- and high tides in the bay and attenuates tidal amplitudes (Godin, 1986; St-Laurent et al., 2008). A study exploring the impacts of possible future accelerated sea ice retreat and the feedbacks on tides would build upon the work presented here.

3.3 Implications of research

Throughout this thesis, it was established that future sea level changes will considerably impact ocean tides in Hudson Bay, but these changes are complex and not immediately intuitive. It is important to capture this nuanced behaviour in order to prepare for the correct sign of change, which will have far reaching consequences. The following discussion explores the human and ecological implications of these changes.

Hudson Strait is the primary marine traffic corridor into the Hudson Bay region and is projected to experience higher volumes of shipping in the future as the length of the open water season increases (Andrews et al., 2016). Changes in tidal amplitudes and resonance in the strait may impact the timing of low and high tides, which would in turn affect navigational routes. Future work on Arctic shipping should take into account the sea level and tide changes presented here in order to assess possible vulnerabilities and opportunities associated with increased marine traffic.

In an audit conducted in 2014 by the Office of the Auditor General of Canada, it was stated that hydrographic survey data of the Canadian Arctic is inadequate and largely outdated, with only 25% of charts in the Canadian Arctic meeting modern standards (Office of the Auditor General of Canada, 2014). This work highlighted the need for accurate, high-resolution bathymetry data for tide modelling, but the implications of inaccurate bathymetric data are far reaching. Northern communities such as those along the periphery of Hudson Bay rely on ocean access for transport and food, and the absence of reliable charts exacerbates the vulnerabilities that these communities face. Furthermore, outdated charts hinder the ability of emergency response efforts to execute search and rescue missions and are hazardous for navigation. At present, the Canadian Coast Guard icebreaker *CGS Amundsen* is the only research vessel that voyages through the Canadian Arctic each year and is equipped with survey instruments for

seabed mapping. To improve the quality of hydrographic data available, it is recommended that these measurement collection efforts continue in future Amundsen expeditions.

The Hudson Bay Lowlands are extensive salt marshes colonizing the intertidal zone surrounding Hudson Bay and are characterized by a diverse community of plant species that provide habitats for migratory bird species and shorebirds (Morrison & Gaston, 1986). Salt marsh development and productivity is intricately linked to sea level and tides, and any changes to water levels exceeding the marsh's adaptation capacity will have implications for the species living in the marsh (Kirwan & Guntenspergen, 2010; Nicholls & Cazenave, 2010). In order to survive, salt marshes must keep pace with the rate of sea level rise (Morris et al., 2002; Kirwan & Guntenspergen, 2010). Salt marshes are also strongly influenced by the tidal regime, with the tidal range controlling the rate salt marsh growth and play an important role in determining the ecosystem's resiliency to future sea level rise (Friedrichs & Perry, 2001; Kirwan & Guntenspergen, 2010; Morris et al., 2002). Findings from this work can be used to identify the most vulnerable regions in the Hudson Bay Lowlands to future sea level and tide changes, such that environmental projection initiatives or defense structures can be implemented. In doing so, biodiversity losses can be minimized.

Coastal changes would have profound impacts on the indigenous communities surrounding Hudson Bay whose lives and livelihoods depend on the natural environment. Under the low-end Antarctic ice loss scenario, glacial isostatic uplift dominates, which could result in the formation of land bridges between present day islands and the mainland. The formation of land bridges in James Bay would be particularly contentious, as the Cree in the region signed a treaty (Treaty Number 9) to relinquish land covered by water, however the treaty did not specify how emergent land would be handled (Tsuji et al., 2009; 2016). Conversely, under the high-end Antarctic ice loss scenario, these communities would face a different set of challenges. Landward migration of the shoreline could jeopardize current infrastructure and limit further development of the built environment. Furthermore, changes in tides may affect the frequency and magnitude of flooding events, leading to an increased need for flood defense structures. The findings from this thesis can help inform coastal management and adaption strategies, that, if developed in partnership with indigenous community members, would lead to effective and judicious decision making.

References

Amante, C. & B.W. Eakins (2009). ETOPO1 1 Arc-Minute Global Relief Model: Procedures, Data Sources and Analysis. NOAA Technical Memorandum NESDIS NGDC-24. National Geophysical Data Center, NOAA. doi:10.7289/V5C8276M

Andrews, J., Babb, D., McKernan, M., Horton, B., & Barber, D. (2016). Climate Change in the Hudson Bay Complex: Opportunities and Vulnerabilities for the Port of Churchill's Marine Operations. *The Centre for Earth Observation Science (CEOS)*. doi: 10.5203/lwbin.ceos.2016.1

Arbic, B., & Garrett, C. (2010). A coupled oscillator model of shelf and ocean tides. *Continental Shelf Research*, *30*(6), 564-574. doi: 10.1016/j.csr.2009.07.008

Arbic, B., Karsten, R., & Garrett, C. (2009). On tidal resonance in the global ocean and the back-effect of coastal tides upon open-ocean tides. *Atmosphere-Ocean*, *47*(4), 239-266. doi: 10.3137/oc311.2009

Arbic, B., MacAyeal, D., Mitrovica, J., & Milne, G. (2004). Ocean tides and Heinrich events. *Nature*, *432*(7016), 460-460. doi: 10.1038/432460a

Arbic, B., St-Laurent, P., Sutherland, G., & Garrett, C. (2007). On the resonance and influence of the tides in Ungava Bay and Hudson Strait. *Geophysical Research Letters*, *34*(17). doi: 10.1029/2007gl030845

Argus, D., Peltier, W., Drummond, R., & Moore, A. (2014). The Antarctica component of postglacial rebound model ICE-6G_C (VM5a) based on GPS positioning, exposure age dating of ice thicknesses, and relative sea level histories. *Geophysical Journal International*, *198*(1), 537-563. doi: 10.1093/gji/ggu140

Becker, J., Sandwell, D., Smith, W., Braud, J., Binder, B., & Depner, J. et al. (2009). Global Bathymetry and Elevation Data at 30 Arc Seconds Resolution: SRTM30_PLUS. *Marine Geodesy*, *32*(4), 355-371. doi: 10.1080/01490410903297766

Chen, X., Zhang, X., Church, J., Watson, C., King, M., & Monselesan, D. et al. (2017). The increasing rate of global mean sea-level rise during 1993–2014. *Nature Climate Change*, *7*(7), 492-495. doi: 10.1038/nclimate3325

Church, J.A., P.U. Clark, A. Cazenave, J.M. Gregory, S. Jevrejeva, A. Levermann, M.A. Merrifield, G.A. Milne, R.S. Nerem, P.D. Nunn, A.J. Payne, W.T. Pfeffer, D. Stammer and A.S. Unnikrishnan, 2013: Sea Level Change. In: Climate Change 2013: The Physical Science Basis. Contribution of Working Group I to the Fifth Assessment Report of the Intergovernmental Panel on Climate Change [Stocker, T.F., D. Qin, G.-K. Plattner, M. Tignor, S.K. Allen, J. Boschung, A. Nauels, Y. Xia, V. Bex and P.M. Midgley (eds.)]. Cambridge University Press, Cambridge, United Kingdom and New York, NY, USA.

Church, J., & White, N. (2011). Sea-Level Rise from the Late 19th to the Early 21st Century. *Surveys In Geophysics*, *32*(4-5), 585-602. doi: 10.1007/s10712-011-9119-1

Clark, J., & Lingle, C. (1977). Future sea-level changes due to West Antarctic ice sheet fluctuations. *Nature*, *269*(5625), 206-209. doi: 10.1038/269206a0

Clark, P., Church, J., Gregory, J., & Payne, A. (2015). Recent Progress in Understanding and Projecting Regional and Global Mean Sea Level Change. *Current Climate Change Reports*, *1*(4), 224-246. doi: 10.1007/s40641-015-0024-4

Clark, P., Dyke, A., Shakun, J., Carlson, A., Clark, J., & Wohlfarth, B. et al. (2009). The Last Glacial Maximum. *Science*, *325*(5941), 710-714. doi: 10.1126/science.1172873

Clark, P., Shakun, J., Marcott, S., Mix, A., Eby, M., & Kulp, S. et al. (2016). Consequences of twenty-first-century policy for multi-millennial climate and sea-level change. *Nature Climate Change*, *6*(4), 360-369. doi: 10.1038/nclimate2923

Clarke, A., & Battisti, D. (1981). The effect of continental shelves on tides. *Deep Sea Research Part A. Oceanographic Research Papers*, *28*(7), 665-682. doi: 10.1016/0198-0149(81)90128-x

Collins, M., R. Knutti, J. Arblaster, J.-L. Dufresne, T. Fichefet, P. Friedlingstein, X. Gao, W.J. Gutowski, T. Johns, G. Krinner, M. Shongwe, C. Tebaldi, A.J. Weaver and M. Wehner, 2013: Long-term Climate Change: Projections, Commitments and Irreversibility. In: Climate Change 2013: The Physical Science Basis. Contribution of Working Group I to the Fifth Assessment Report of the Intergovernmental Panel on Climate Change [Stocker, T.F., D. Qin, G.-K. Plattner, M. Tignor, S.K. Allen, J. Boschung, A. Nauels, Y. Xia, V. Bex and P.M. Midgley (eds.)]. Cambridge University Press, Cambridge, United Kingdom and New York, NY, USA.

Craft, C., Clough, J., Ehman, J., Joye, S., Park, R., & Pennings, S. et al. (2009). Forecasting the effects of accelerated sea-level rise on tidal marsh ecosystem services. *Frontiers In Ecology And The Environment*, *7*(2), 73-78. doi: 10.1890/070219

DeConto, R., & Pollard, D. (2016). Contribution of Antarctica to past and future sea-level rise. *Nature*, *531*(7596), 591-597. doi: 10.1038/nature17145

Denton, G., Anderson, R., Toggweiler, J., Edwards, R., Schaefer, J., & Putnam, A. (2010). The Last Glacial Termination. *Science*, *328*(5986), 1652-1656. doi: 10.1126/science.1184119

Drinkwater, K. (1986). Chapter 13 Physical Oceanography of Hudson Strait and Ungava Bay. In *Canadian Inland Seas*, 237-264. Elsevier Oceanographic Series. doi: 10.1016/s0422-9894(08)70906-1 s

Dyke, A. (2004). An outline of North American deglaciation with emphasis on central and northern Canada. *Quaternary Glaciations-Extent And Chronology - Part II: North America*, 373-424. doi: 10.1016/s1571-0866(04)80209-4

Dziewonski, A., & Anderson, D. (1981). Preliminary reference Earth model. *Physics Of The Earth And Planetary Interiors*, *25*(4), 297-356. doi: 10.1016/0031-9201(81)90046-7

Edwards, T., Brandon, M., Durand, G., Edwards, N., Golledge, N., & Holden, P. et al. (2019). Revisiting Antarctic ice loss due to marine ice-cliff instability. *Nature*, *566*(7742), 58-64. doi: 10.1038/s41586-019-0901-4

Egbert, G., Bennett, A., & Foreman, M. (1994). TOPEX/POSEIDON tides estimated using a global inverse model. *Journal of Geophysical Research*, *99*(C12), 24821. doi: 10.1029/94jc01894

Egbert, G., & Erofeeva, S. (2002). Efficient Inverse Modeling of Barotropic Ocean Tides. *Journal Of Atmospheric And Oceanic Technology*, *19*(2), 183-204. doi: 10.1175/1520-0426(2002)019<0183:eimobo>2.0.co;2

Egbert, G., & Ray, R. (2001). Estimates of M2 tidal energy dissipation from TOPEX/Poseidon altimeter data. *Journal Of Geophysical Research: Oceans*, *106*(C10), 22475-22502. doi: 10.1029/2000jc000699

Egbert, G., Ray, R., & Bills, B. (2004). Numerical modeling of the global semidiurnal tide in the present day and in the last glacial maximum. *Journal Of Geophysical Research: Oceans*, *109*(C3). doi: 10.1029/2003jc001973

Forrester, W.D. (1983). *Canadian Tide Manual*. Department of Fisheries and Oceans, Canadian Hydrographic Service, Ottawa

Forsberg, R., Sørensen, L., & Simonsen, S. (2017). Greenland and Antarctica Ice Sheet Mass Changes and Effects on Global Sea Level. *Surveys In Geophysics*, *38*(1), 89-104. doi: 10.1007/s10712-016-9398-7

Friedrichs, C. T., & Perry, J. E. (2001). Tidal salt marsh morphodynamics: A synthesis. Journal of Coastal Research, 27(27), 7–37.

Godin, G. (1986). Modification by an Ice Cover of the Tide in James Bay and Hudson Bay. *ARCTIC*, *39*(1). doi: 10.14430/arctic2048

Golledge, N., Keller, E., Gomez, N., Naughten, K., Bernales, J., Trusel, L., & Edwards, T. (2019). Global environmental consequences of twenty-first-century ice-sheet melt. *Nature*, *566*(7742), 65-72. doi: 10.1038/s41586-019-0889-9

Golledge, N., Kowalewski, D., Naish, T., Levy, R., Fogwill, C., & Gasson, E. (2015). The multi-millennial Antarctic commitment to future sea-level rise. *Nature*, *526*(7573), 421-425. doi: 10.1038/nature15706

Gomez, N., Mitrovica, J., Tamisiea, M., & Clark, P. (2010). A new projection of sea level change in response to collapse of marine sectors of the Antarctic Ice Sheet. *Geophysical Journal International*, *180*(2), 623-634. doi: 10.1111/j.1365-246x.2009.04419.x

Gough, W.A. (1998). Projections of sea-level change in Hudson and James Bays, Canada, due to global warming. Arctic and Alpine Research 30(1):84 – 88. doi: 10.2307/1551748

Green, J. (2010). Ocean tides and resonance. *Ocean Dynamics*, *60*(5), 1243-1253. doi: 10.1007/s10236-010-0331-1

Green, J., & Nycander, J. (2013). A Comparison of Tidal Conversion Parameterizations for Tidal Models. *Journal Of Physical Oceanography*, *43*(1), 104-119. doi: 10.1175/jpo-d-12-023.1

Hay, C., Morrow, E., Kopp, R., & Mitrovica, J. (2015). Probabilistic reanalysis of twentieth-century sea-level rise. *Nature*, *517*(7535), 481-484. doi: 10.1038/nature14093

IPCC, 2014: Climate Change 2014: Impacts, Adaptation, and Vulnerability. Summaries, Frequently Asked Questions, and Cross-Chapter Boxes. A Contribution of Working Group II to the Fifth Assessment Report of the Intergovernmental Panel on Climate Change [Field, C.B., V.R. Barros, D.J. Dokken, K.J. Mach, M.D. Mastrandrea, T.E. Bilir, M. Chatterjee, K.L. Ebi, Y.O. Estrada, R.C. Genova, B. Girma, E.S. Kissel, A.N. Levy, S. MacCracken,P.R. Mastrandrea, and L.L. White (eds.)]. World Meteorological Organization, Geneva, Switzerland, 190 pp.

Jevrejeva, S., Jackson, L., Riva, R., Grinsted, A., & Moore, J. (2016). Coastal sea level rise with warming above 2 °C. *Proceedings of The National Academy Of Sciences*, *113*(47), 13342-13347. doi: 10.1073/pnas.1605312113

Jevrejeva, S., Moore, J., Grinsted, A., Matthews, A., & Spada, G. (2014). Trends and acceleration in global and regional sea levels since 1807. *Global And Planetary Change*, *113*, 11-22. doi: 10.1016/j.gloplacha.2013.12.004

Kendall, R., Mitrovica, J., & Milne, G. (2005). On post-glacial sea level - II. Numerical formulation and comparative results on spherically symmetric models. *Geophysical Journal International*, *161*(3), 679-706. doi: 10.1111/j.1365-246x.2005.02553.x

Kirwan, M., & Guntenspergen, G. (2010). Influence of tidal range on the stability of coastal marshland. *Journal of Geophysical Research: Earth Surface*, *115*(F2). doi: 10.1029/2009jf001400

Kirwan, M., & Megonigal, J. (2013). Tidal wetland stability in the face of human impacts and sea-level rise. *Nature*, *504*(7478), 53-60. doi: 10.1038/nature12856

Kirwan, M., Guntenspergen, G., D'Alpaos, A., Morris, J., Mudd, S., & Temmerman, S. (2010). Limits on the adaptability of coastal marshes to rising sea level. *Geophysical Research Letters*, *37*(23), n/a-n/a. doi: 10.1029/2010gl045489

Kleptsova, O., & Pietrzak, J. (2018). High resolution tidal model of Canadian Arctic Archipelago, Baffin and Hudson Bay. *Ocean Modelling*, *128*, 15-47. doi: 10.1016/j.ocemod.2018.06.001

Kopp, R., DeConto, R., Bader, D., Hay, C., Horton, R., & Kulp, S. et al. (2017). Evolving Understanding of Antarctic Ice-Sheet Physics and Ambiguity in Probabilistic Sea-Level Projections. *Journal of Geophysical Research: Earth's Future*, *5*(12), 1217-1233. doi: 10.1002/2017ef000663

Lee, H. (1960). Late Glacial and Postglacial Hudson Bay Sea Episode. *Science*, *131*(3413), 1609-1611. doi: 10.1126/science.131.3413.1609

Lemmen, D.S. and Warren, F.J. (2016): Synthesis; *in* Canada's Marine Coasts in a Changing Climate, (ed.) D.S. Lemmen, F.J. Warren, T.S. James and C.S.L. Mercer Clarke; Government of Canada, Ottawa, ON, p. 17-26.

Meinshausen, M., Smith, S., Calvin, K., Daniel, J., Kainuma, M., & Lamarque, J. et al. (2011). The RCP greenhouse gas concentrations and their extensions from 1765 to 2300. *Climatic Change*, *109*(1-2), 213-241. doi: 10.1007/s10584-011-0156-z

Milne, G., & Mitrovica, J. (1998). Postglacial sea-level change on a rotating Earth. *Geophysical Journal International*, *133*(1), 1-19. doi: 10.1046/j.1365-246x.1998.1331455.x

Mitrovica, J., Gomez, N., & Clark, P. (2009). The Sea-Level Fingerprint of West Antarctic Collapse. *Science*, *323*(5915), 753-753. doi: 10.1126/science.1166510

Mitrovica, J., Gomez, N., Morrow, E., Hay, C., Latychev, K., & Tamisiea, M. (2011). On the robustness of predictions of sea level fingerprints. *Geophysical Journal International*, *187*(2), 729-742. doi: 10.1111/j.1365-246x.2011.05090.x

Mitrovica, J., & Milne, G. (2003). On post-glacial sea level: I. General theory. *Geophysical Journal International*, *154*(2), 253-267. doi: 10.1046/j.1365-246x.2003.01942.x

Mitrovica, J., Tamisiea, M., Davis, J., & Milne, G. (2001). Recent mass balance of polar ice sheets inferred from patterns of global sea-level change. *Nature*, *409*(6823), 1026-1029. doi: 10.1038/35059054

Moore, J., Grinsted, A., Zwinger, T., & Jevrejeva, S. (2013). Semiempirical and process-based global sea level projections. *Reviews of Geophysics*, *51*(3), 484-522. doi: 10.1002/rog.20015

Morris, J., Sundareshwar, P., Nietch, C., Kjerfve, B., & Cahoon, D. (2002). Responses of coastal wetlands to rising sea level. *Ecology*, *83*(10), 2869-2877. doi: 10.1890/0012-9658(2002)083[2869:rocwtr]2.0.co;2

Morrison, R., & Gaston, A. (1986). Chapter 18 Marine and Coastal Birds of James Bay, Hudson Bay, and Foxe Basin. In *Canadian Inland Seas*, 355-386. Elsevier Oceanographic Series. doi: 10.1016/S0422-9894

Moss, R., Babiker, M., Brinkman, S., Calvo,E., Carter, T.R., Edmonds, J., Elgizouli I, Emori S, Erda L, Hibbard K, Jones R, Kainuma M, Kelleher J, Lamarque J-F, Manning MR, Matthews B, Meehl J, Meyer L, Mitchell JFB, Nakicenovic N, O'Neill B, Pichs R, Riahi K, Rose SK, Runci P, Stouffer RJ, van Vuuren DP, Weyant JP, Wilbanks TJ, van Ypersele JP, Zurek M (2008) Towards new scenarios for analysis of emissions, climate change, impacts, and response strategies: IPCC Expert Meeting Report, 19–21 September 2007. Noordwijkerhout, The Netherlands, pp 155

Moss, R., Edmonds JA, Hibbard KA, Manning MR, Rose SK, van Vuuren DP, Carter TR, Emori S, Kainuma M, Kram T, Meehl GA, Mitchell JFB, Nakicenovic N, Riahi K, Smith SJ, Stouffer RJ, Thomson AM, Weyant JP, Wilbanks TJ (2010) The next generation of scenarios for climate change research and assessment. Nature 463(7282):747–756

Nerem, R., Beckley, B., Fasullo, J., Hamlington, B., Masters, D., & Mitchum, G. (2018). Climate-change–driven accelerated sea-level rise detected in the altimeter era. *Proceedings of The National Academy of Sciences*, *115*(9), 2022-2025. doi: 10.1073/pnas.1717312115

Nicholls, R., & Cazenave, A. (2010). Sea-Level Rise and Its Impact on Coastal Zones. *Science*, *328*(5985), 1517-1520. doi: 10.1126/science.1185782

Office of the Auditor General of Canada. (2014). *Report of the Commissioner of the Environment and Sustainable Development – Chapter 3: Marine Navigation in the Canadian Arctic*. Retrieved from http://www.oag-bvg.gc.ca/internet/English/parl_cesd_201410_03_e_39850.html

O'Reilly, C. T., R. Solvason, and C. Solomon (2005), Where are the world's largest tides?, in BIO Annual Report ''2004 in Review,'' edited by J. Ryan, pp. 44 – 46, Biotechnol. Ind. Org., Washington, D. C.

Padman, L., Siegfried, M., & Fricker, H. (2018). Ocean Tide Influences on the Antarctic and Greenland Ice Sheets. *Reviews of Geophysics*, *56*(1), 142-184. doi: 10.1002/2016rg000546

Peltier, W. (1999). Global sea level rise and glacial isostatic adjustment. *Global And Planetary Change*, *20*(2-3), 93-123. doi: 10.1016/s0921-8181(98)00066-6

Peltier, W. (2004). Global glacial isostasy and the surface of the ice-age Earth: the ICE-5G (VM2) model and GRACE. *Annual Review of Earth and Planetary Sciences*, *32*(1), 111-149. doi: 10.1146/annurev.earth.32.082503.144359

Peltier, W., Argus, D., & Drummond, R. (2015). Space geodesy constrains ice age terminal deglaciation: The global ICE-6G_C (VM5a) model. *Journal of Geophysical Research: Solid Earth*, *120*(1), 450-487. doi: 10.1002/2014jb011176

Pollard, D., Gomez, N., & Deconto, R. (2017). Variations of the Antarctic Ice Sheet in a Coupled Ice Sheet-Earth-Sea Level Model: Sensitivity to Viscoelastic Earth Properties. *Journal of Geophysical Research: Earth Surface*, *122*(11), 2124-2138. doi: 10.1002/2017jf004371

Pugh, D., & Woodworth, P. (2014). *Sea-level science: understanding tides, surges, tsunamis and mean sea-level changes*. Cambridge University Press.

Ross, A., Najjar, R., Li, M., Lee, S., Zhang, F., & Liu, W. (2017). Fingerprints of Sea Level Rise on Changing Tides in the Chesapeake and Delaware Bays. *Journal of Geophysical Research: Oceans*, *122*(10), 8102-8125. doi: 10.1002/2017jc012887

Simon, K., James, T., Henton, J., & Dyke, A. (2016). A glacial isostatic adjustment model for the central and northern Laurentide Ice Sheet based on relative sea level and GPS measurements. *Geophysical Journal International*, *205*(3), 1618-1636. doi: 10.1093/gji/ggw103

Slangen, A., Adloff, F., Jevrejeva, S., Leclercq, P., Marzeion, B., Wada, Y., & Winkelmann, R. (2016). A Review of Recent Updates of Sea-Level Projections at Global and Regional Scales. *Surveys in Geophysics*, *38*(1), 385-406. doi: 10.1007/s10712-016-9374-2

Stammer, D., Ray, R., Andersen, O., Arbic, B., Bosch, W., & Carrère, L. et al. (2014). Accuracy assessment of global barotropic ocean tide models. *Reviews of Geophysics*, *52*(3), 243-282. doi: 10.1002/2014rg000450

Stewart, D.B., and Lockhart, W.L. (2005). *An Overview of the Hudson Bay Marine Ecosystem*. Canadian technical report of fisheries and aquatic sciences no. 2586. Retrieved from Government of Canada, Department of Fisheries and Oceans website: http://www.dfo-mpo.gc.ca/libraries- bibliotheques/toc-tdm/314704-eng.htm

St-Laurent, P., Saucier, F., & Dumais, J. (2008). On the modification of tides in a seasonally ice-covered sea. *Journal of Geophysical Research*, *113*(C11). doi: 10.1029/2007jc004614

Tamisiea, M., & Mitrovica, J. (2011). The Moving Boundaries of Sea Level Change: Understanding the Origins of Geographic Variability. *Oceanography*, *24*(2), 24-39. doi: 10.5670/oceanog.2011.2

Tsuji, L.J.S., Gomez, N., Mitrovica, J.X., and Kendall, R. (2009). Post-glacial isostatic adjustment and global warming in Subarctic Canada: Implications for islands of the James Bay region. Arctic 62(4):458 – 467. doi: 10.14430/arctic176

Tsuji, L., Daradich, A., Gomez, N., Hay, C., & Mitrovica, J. (2016). Sea Level Change in the Western James Bay Region of Subarctic Ontario: Emergent Land and Implications for Treaty No. 9. Arctic, 69(1), 99. doi: 10.14430/arctic4542

Uehara, K., Scourse, J., Horsburgh, K., Lambeck, K., & Purcell, A. (2006). Tidal evolution of the northwest European shelf seas from the Last Glacial Maximum to the present. *Journal Of Geophysical Research*, *111*(C9). doi: 10.1029/2006jc003531

Weatherall, P., Marks, K., Jakobsson, M., Schmitt, T., Tani, S., & Arndt, J. et al. (2015). A new digital bathymetric model of the world's oceans. *Earth and Space Science*, *2*(8), 331-345. doi: 10.1002/2015ea000107

Webb, D. (2014). On the tides and resonances of Hudson Bay and Hudson Strait. *Ocean Science*, *10*(3), 411-426. doi: 10.5194/os-10-411-2014

Wilmes, S. (2016). *The impact of large-scale sea-level changes on tides in the past, present and future* (Ph.D). Bangor University.

Wilmes, S., Green, J., Gomez, N., Rippeth, T., & Lau, H. (2017). Global Tidal Impacts of Large-Scale Ice Sheet Collapses. *Journal of Geophysical Research: Oceans*, *122*(11), 8354-8370. doi: 10.1002/2017jc013109

Wingham, D., Wallis, D., & Shepherd, A. (2009). Spatial and temporal evolution of Pine Island Glacier thinning, 1995–2006. *Geophysical Research Letters*, *36*(17). doi: 10.1029/2009gl039126

Winkelmann, R., Martin, M., Haseloff, M., Albrecht, T., Bueler, E., Khroulev, C., & Levermann, A. (2011). The Potsdam Parallel Ice Sheet Model (PISM-PIK) – Part 1: Model description. *The Cryosphere*, *5*(3), 715-726. doi: 10.5194/tc-5-715-2011

Woodward, R. (1888), On the form of and position of mean sea level, *U.S. Geol. Surv. Bull*., 48, 87–170.

WRCP Global Sea Level Budget Group. Global sea-level budget 1993–present. (2018). *Earth System Science Data*, *10*(3), 1551-1590. doi: 10.5194/essd-10-1551-2018